nature neuroscience

ARTICLES

https://doi.org/10.1038/s41593-019-0405-4

A subcortical excitatory circuit for sensory-triggered predatory hunting in mice

Congping Shang[1,2,7], Aixue Liu[2,3,7], Dapeng Li[2,7], Zhiyong Xie[2,7], Zijun Chen[4,5], Meizhu Huang[2], Yang Li[2], Yi Wang[4], Wei L. Shen[6] and Peng Cao[2,3*]

Predatory hunting plays a fundamental role in animal survival. Little is known about the neural circuits that convert sensory cues into neural signals to drive this behavior. Here we identified an excitatory subcortical neural circuit from the superior colliculus to the zona incerta that triggers predatory hunting. The superior colliculus neurons that form this pathway integrate motion-related visual and vibrissal somatosensory cues of prey. During hunting, these neurons send out neural signals that are temporally correlated with predatory attacks, but not with feeding after prey capture. Synaptic inactivation of this pathway selectively blocks hunting for prey without impairing other sensory-triggered behaviors. These data reveal a subcortical neural circuit that is specifically engaged in translating sensory cues into neural signals to provoke predatory hunting.

As an evolutionarily conserved behavior, predatory hunting has been the focus of studies using diverse animal models[1–6]. Pioneering neuroethological studies led by Ewert[1] of prey-capture behavior in toads have raised the concept of feature detection, whereby functional units in the optic tectum extract prey-derived visual cues and drive prey capture[1]. However, it is unclear how the mammalian brain detects prey-derived sensory cues and trigger prey-capture behavior. The availability of molecular tools to analyze neural circuits seems to provide an opportunity to address this question[7,8].

The superior colliculus (SC), a mammalian homolog of the optic tectum, is a midbrain structure for sensory information processing[9,10], sensorimotor transformation[11] and cognitive functions[12]. The superficial layers of the SC primarily receive visual inputs from the retina and visual cortex[13–15]. Meanwhile, SC neurons in the intermediate and deep layers process information of visual, somatosensory and auditory modalities[16–19]. The SC of rats has been implicated in predatory hunting, as evidenced by an impairment of prey-capture behavior after SC lesion[20]. Moreover, predatory hunting induces a large increase in Fos expression in the intermediate layer of the lateral SC[21]. These observations suggest that the feature-detection neurons for prey-capture behavior may exist in the SC of mammalian brains.

Here, by combining genetically encoded circuit analysis tools, we identified a subset of SC neurons that are critical for predatory hunting in mice. These neurons respond to motion-related visual and somatosensory cues from prey. During predatory hunting, they send motor signals to the zona incerta (ZI) for driving predatory attack. These data reveal how the brain transforms prey-derived sensory cues into predatory attack during prey-capture behavior.

Results

We began this study by setting up a behavioral paradigm to quantitatively analyze predatory hunting in mice. The hunting test began with the introduction of a cockroach (prey) to a mouse (predator) in an arena (Fig. 1a). Mouse behavior was recorded using three orthogonally positioned cameras. The overhead camera recorded the instantaneous positions of the predator and prey, with which we measured the locomotion speed of the predator (Supplementary Fig. 1a) and the prey–predator distance (PPD) (Supplementary Video 1; Supplementary Fig. 1b, upper). The PPD oscillated over time and finally reached zero, indicating the capture of the prey. The two horizontal cameras monitored the jaw attacks of the predator (Supplementary Video 2) marked in parallel with the PPD time course (Supplementary Fig. 1b, lower). The last attack that led to prey capture ended the hunting phase and switched the mouse behavior to feeding. The behavioral ethogram of predatory hunting (Supplementary Fig. 1b) enabled us to quantify hunting efficiency by measuring the latency to attack (time from initiation to the first jaw attack; 14 ± 2.1 s, $n = 24$ mice), time to capture (time from initiation to the last jaw attack; 58 ± 7.2 s, $n = 24$ mice) and attack frequency (number of attacks divided by time to capture; 0.72 ± 0.11 Hz, $n = 24$ mice).

With this paradigm, we assessed the role of the SC in predatory hunting by globally silencing SC neurons with tetanus neurotoxin (TeNT), a molecular tool for synaptic inactivation. The effectiveness and specificity of TeNT-mediated synaptic inactivation of SC neurons were validated (Supplementary Fig. 2). Then we injected the adeno-associated virus (AAV) vector AAV-DJ-hSyn-EGFP-2A-TeNT bilaterally into the SC (Supplementary Fig. 3a), resulting in the expression of enhanced green fluorescent protein (EGFP) and TeNT in SC neurons (Supplementary Fig. 3b; infection rate of $93 \pm 8\%$, $n = 7$ mice). SC inactivation did not significantly influence the basal locomotor behaviors of mice that explored the arena (Supplementary Fig. 3c–e). However, it strongly impaired the predatory hunting behavior of these mice (Supplementary Fig. 3f), confirming the critical role of the SC in predatory hunting in rodents[20,21].

FosTRAP strategy to label hunting-associated SC neurons and their projections. To identify the key neurons in the SC for predatory hunting, we employed the FosTRAP strategy[22] to genetically

[1]Peking University–Tsinghua University–NIBS Joint Graduate Program, School of Life Sciences, Tsinghua University, Beijing, China. [2]National Institute of Biological Sciences, Beijing, China. [3]Graduate School of Peking Union Medical College, Chinese Academy of Medical Sciences, Beijing, China. [4]State Key Laboratory of Brain and Cognitive Sciences, Institute of Biophysics, Chinese Academy of Sciences, Beijing, China. [5]University of Chinese Academy of Sciences, Beijing, China. [6]School of Life Science and Technology, ShanghaiTech University, Shanghai, China. [7]These authors contributed equally: Congping Shang, Aixue Liu, Dapeng Li and Zhiyong Xie. *e-mail: caopeng@nibs.ac.cn

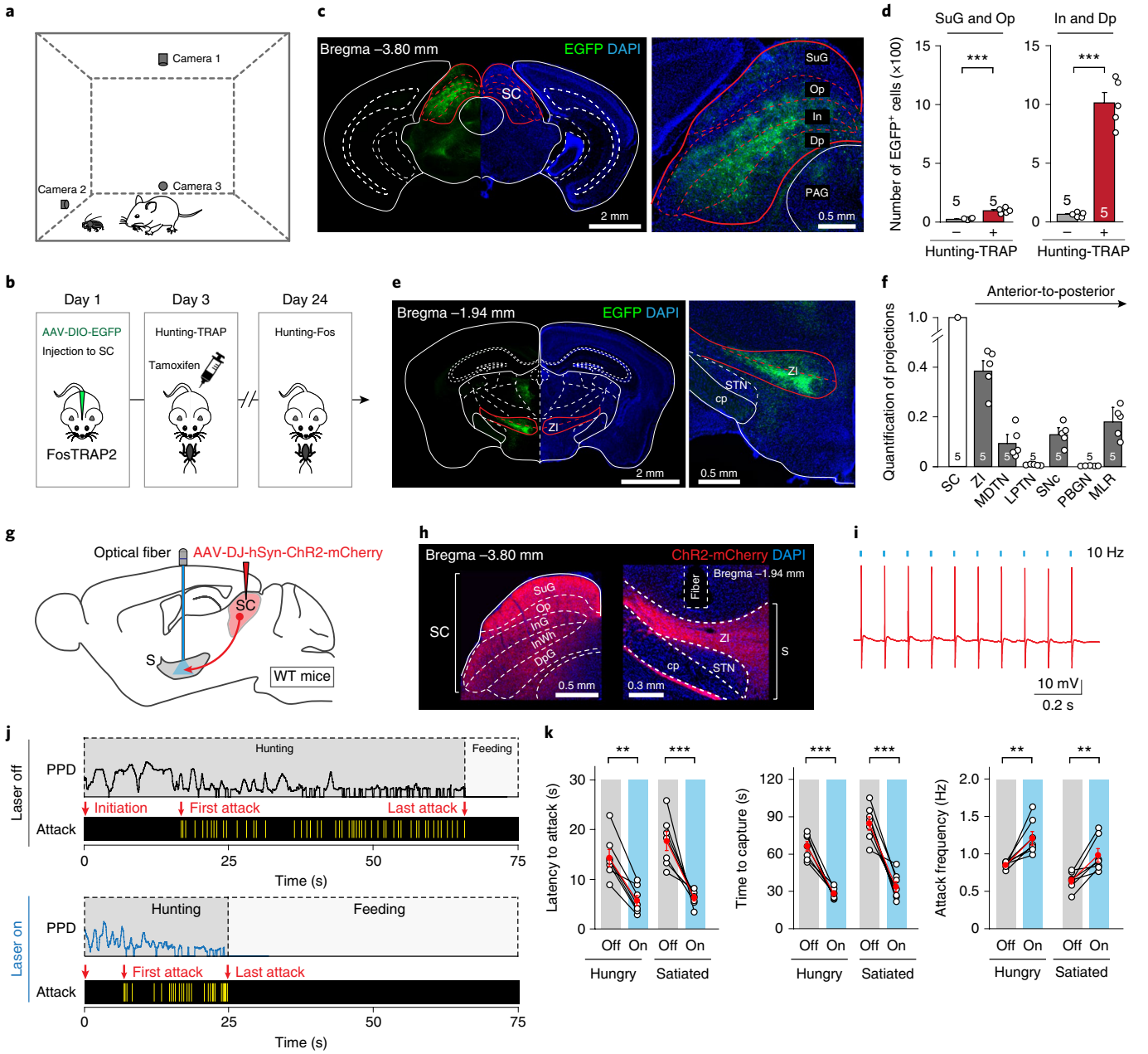

Fig. 1 | Activation of the SC–S pathway provokes predatory hunting. a, Schematic of the behavioral paradigm to monitor predatory hunting in mice. **b**, Schematic of the FosTrap procedure. **c**, An example coronal section (left) and the magnified area of the SC (right) showing the EGFP$^+$ hunting-associated SC neurons in different SC layers. **d**, Number of EGFP$^+$ cells in different layers of the SC with and without Hunting-TRAP. **e**, An example coronal section (left) and the magnified area of EGFP$^+$ hunting-associated SC projections to the ZI (right). **f**, Quantification of EGFP$^+$ axonal projections of hunting-associated SC neurons labeled by Hunting-TRAP. The fluorescence of each projection was normalized to the average fluorescence in the SC. MDTN, medial posterior tuberal nucleus; LPTN, lateral posterior tuberal nucleus; PBGN, parabigeminal nucleus; SNc, substantia nigra pars compacta. **g**, Schematic of injection of AAV-DJ-hSyn-ChR2-mCherry into the SC followed by optical fiber implantation above the subthalamus for activation of the SC–S pathway. **h**, Example micrographs showing ChR2-mCherry expression in the SC (left) and the optical fiber track above ChR2-mCherry$^+$ axon terminals in the ZI and STN, two major nuclei of the subthalamus (right). The experiment was independently repeated with similar results in $n = 7$ mice. **i**, Light-pulse trains (473 nm, 2 ms, 10 Hz, 20 mW) reliably evoked phase-locked spiking activity in ChR2-mCherry$^+$ SC cells. The experiment was independently repeated five times with similar results obtained. **j**,**k**, Example behavioral ethograms of hungry mice (**j**) and quantitative analyses (**k**) of latency to attack, time to capture and attack frequency of mice with (On) or without (Off) optogenetic activation of the SC–S pathway. The same mice were tested in both hungry and satiated states ($n = 7$ mice). The numbers of mice used in the experiments are indicated in the graphs (**d**, **f** and **k**). Data in **d**, **f** and **k** are the mean ± s.e.m. (error bars). Statistical analyses in **d** and **k** were performed using two-sided Student *t*-tests (**$P < 0.01$, ***$P < 0.001$). The broken and unbroken red and white lines in section images (**c**, **e**, **h**) represent boundaries of brain regions. The red lines in **k** represent the averaged data. cp, cerebral peduncle; Dp, deep layer; DpG, deep gray layer; In, intermediate layer; InG and InWh, intermediate gray and white layers, respectively; Op, optic nerve layer; SuG, superficial gray layer.

label SC neurons that were activated during predatory hunting. On day 1, we injected AAV-DJ-EF1α-DIO-EGFP unilaterally into the SC of FosTRAP2 mice (Fig. 1b). On day 3, FosTRAP2 mice were treated with tamoxifen and allowed to hunt for 1 h in the home cage (Hunting-TRAP). On day 24, FosTRAP2 mice were allowed to hunt again before perfusion (Hunting-Fos). This procedure resulted in

the labeling of a number of EGFP$^+$ SC neurons (1,103 ± 92 cells, $n = 5$ mice) that were preferentially distributed in the intermediate and deep layers of the SC (Fig. 1c,d). By contrast, far fewer EGFP$^+$ neurons (83 ± 10, $n = 5$ mice) were labeled in control mice without Hunting-TRAP (Supplementary Fig. 4a). To examine the specificity and efficiency of EGFP labeling, we co-immunostained Fos and EGFP in the same SC sections (Supplementary Fig. 4b–d) and found that a large proportion of EGFP$^+$ cells (74 ± 2.1%, $n = 5$ mice) were positive for Fos, whereas a number of Fos$^+$ cells (54 ± 2.3%, $n = 5$ mice) were positive for EGFP. These data indicate that the specificity and efficiency of the FosTRAP procedure to label hunting-associated SC neurons were acceptable. The hunting-associated SC neurons divergently projected to several brain areas, among which the ZI in the subthalamus was the most heavily innervated target (Fig. 1e,f; Supplementary Fig. 4e). These morphological observations suggested an important role of the SC–subthalamus (SC–S) pathway in predatory hunting.

Activation of the SC–S pathway provokes predatory hunting. In subsequent experiments, we focused on dissecting the role of the SC–S pathway in predatory hunting. We first examined whether activation of this pathway provoked hunting. AAV-DJ-hSyn-ChR2-mCherry[23] was injected into the SC, followed by implantation of an optical fiber above ChR2-mCherry$^+$ axon terminals in the subthalamus, which contains the ZI and the adjacent subthalamic nucleus (STN) (Fig. 1g,h). A light-pulse train (473 nm, 2 ms, 20 mW, 10 Hz) reliably evoked phase-locked spiking activity from SC neurons expressing ChR2-mCherry (Fig. 1i). Strikingly, photostimulation of ChR2-mCherry$^+$ axon terminals in the subthalamus provoked predatory hunting (Supplementary Video 3). Quantitative analyses indicated that SC–S pathway activation strongly promoted hunting efficiency by reducing the latency to hunt, decreasing the time to capture and increasing the frequency of attack in both hungry and satiated mice (Fig. 1j,k). The effects of SC–S pathway activation on hunting efficiency depended on the laser power and the frequency and epoch of light stimulation (Supplementary Fig. 5a–c). In control mice injected with AAV-DJ-hSyn-mCherry in the SC, the efficiency of predatory hunting was not altered by light illumination on the SC–S pathway (Supplementary Fig. 5d). As a positive control, photostimulation of hunting-associated SC neurons that expressed ChR2-mCherry also significantly promoted hunting efficiency (Supplementary Fig. 4f,g).

To assess the specificity of the hunting behavior evoked by SC–S pathway activation, we performed additional experiments. First, in an arena with both food pellets and prey, SC–S pathway activation selectively provoked predatory attack to prey rather than induced food consumption (Supplementary Video 4; Supplementary Fig. 5e,f), suggesting that activation of the SC–S pathway specifically evoked hunting rather than a general consummatory behavior. Second, in an arena with both prey and conspecifics, SC–S pathway activation provoked predatory attacks to prey rather than social aggression to conspecifics (Supplementary Video 5; Supplementary Fig. 5g,h), suggesting that the hunting behavior evoked by SC–S pathway activation is not caused by increasing the level of aggression. Third, we examined whether SC–S pathway activation promoted object-exploration behavior[24]. However, SC–S pathway activation did not promote object-exploration behavior (Supplementary Fig. 5i,j). These analyses indicate that SC–S pathway activation specifically induced predatory hunting.

We also examined mouse behavior evoked by activation of the SC–S pathway in the absence of prey. In an arena with regular bedding material (Supplementary Fig. 5k), SC–S pathway activation induced a hunting-like posture in the mouse, with its nose tip tilted toward the bedding (Supplementary Video 6). With this posture, the mouse then actively dug and searched the bedding and occasionally picked up bedding for gnawing (Supplementary Video 6; Supplementary Fig. 5l). These data suggested that even in the absence of prey, SC–S pathway activation may induce motor actions related to prey capture.

The SC–S pathway is selectively required for predatory hunting. Next, we examined whether the SC–S pathway is selectively required for predatory hunting. To inactivate the SC–S pathway, we bilaterally injected AAV-DJ-EF1α-DIO-EGFP-2A-TeNT and AAV2-retro-EF1α-mCherry-IRES-Cre[25] into the SC and subthalamus, respectively, of wild-type (WT) mice (Fig. 2a). In control experiments, we confirmed the dependence of AAV-DJ-EF1α-DIO-EGFP-2A-TeNT on Cre recombinase. We also validated the effectiveness of AAV2-retro-EF1α-mCherry-IRES-Cre to retrogradely label a pathway (Supplementary Fig. 6). The injection of AAV2-retro-EF1α-mCherry-IRES-Cre in the subthalamus (Fig. 2b) and AAV-DJ-EF1α-DIO-EGFP-2A-TeNT in the SC cooperatively labeled subthalamus-projecting SC neurons with EGFP (Fig. 2c), as demonstrated by the co-expression of mCherry and EGFP in the same SC neurons (Fig. 2d). Notably, these subthalamus-projecting SC neurons were localized in the intermediate and deep layers of the lateral SC (Fig. 2c). We found that TeNT expression in the subthalamus-projecting SC neurons significantly reduced the hunting efficiency of the mice (Fig. 2e,f; Supplementary Video 7). However, the same mice did not exhibit deficits in escape behavior triggered by looming stimuli (Fig. 2g,h; Supplementary Video 8). Moreover, SC–S pathway inactivation did not influence daily food intake in mice, suggesting that the SC–S pathway may not regulate motivation for daily food consumption (Fig. 2i). Inactivation of the SC–S pathway also did not significantly alter the object-exploration behavior of mice (Supplementary Fig. 6f,g). Thus, these 'loss-of-function' data suggest that the SC–S pathway is selectively required for predatory hunting.

Characterizations of subthalamus-projecting SC neurons. Then we characterized the subthalamus-projecting SC neurons. Unilateral injection of CTB-555 into the subthalamus of WT mice labeled a subset of neurons localized in the intermediate and deep layers of the lateral SC (Fig. 3a,b; Supplementary Fig. 7). By using primary antibodies that specifically recognize GABA and glutamate, we found that most of the CTB-555$^+$ cells were immunohistochemically glutamate$^+$ (93 ± 5%, $n = 5$ mice) and GABA$^-$ (94 ± 2%, $n = 5$ mice), suggesting that the SC–S pathway is predominantly glutamatergic (Fig. 3c,d). We also examined whether the subthalamus-projecting SC neurons send collaterals to the periaqueductal gray (PAG). CTB-555 and CTB-488 were injected into the subthalamus and PAG of the same mice (Supplementary Fig. 8a,b). Very few SC cells were co-labeled with CTB-555 and CTB-488 (Supplementary Fig. 8c–h), indicating that the subthalamus-projecting SC neurons do not simultaneously project to the PAG.

To examine the physiological properties of subthalamus-projecting SC neurons, we injected AAV2-retro-EF1α-DIO-EGFP into the subthalamus of *vGlut2*-IRES-Cre mice (Supplementary Fig. 9a). This strategy resulted in the labeling of subthalamus-projecting SC neurons with EGFP, which were predominantly glutamate$^+$ and GABA$^-$ (Supplementary Fig. 9b,c). In acute SC slices, these EGFP-labeled SC neurons showed spiking activity with a slow adaptation pattern to depolarizing current injections (Fig. 3e,f).

To examine whether the subthalamus-projecting glutamate$^+$ SC neurons constitute the key circuit module that provokes hunting, we injected AAV-DJ-EF1α-DIO-ChR2-mCherry into the SC of *vGlut2*-IRES-Cre mice, followed by optical fiber implantation above the subthalamus (Fig. 3g). The specific targeting of ChR2-mCherry to glutamate$^+$ SC neurons was confirmed by immunohistochemistry (Fig. 3h; Supplementary Fig. 10a,b) and slice physiology analyses (Supplementary Fig. 10c,d). A light-pulse train (473 nm, 2 ms, 10 Hz, 20 mW) reliably evoked phase-locked spiking activity in

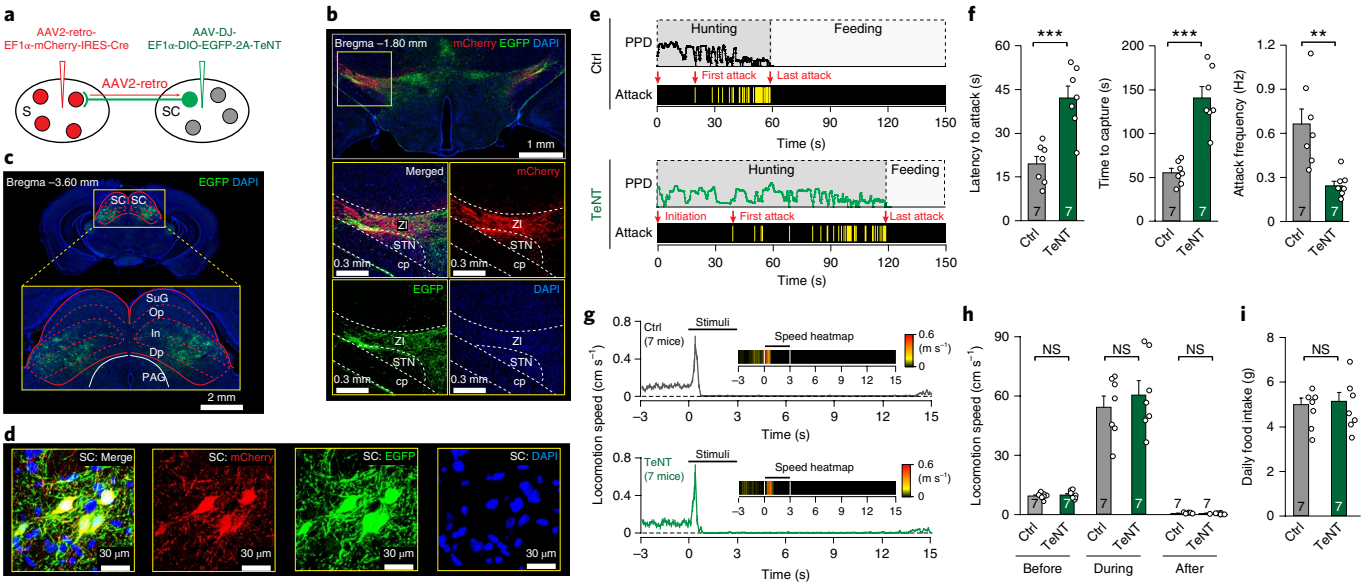

Fig. 2 | The SC–S pathway is selectively required for predatory hunting. a, Schematic of the strategy used to selectively inactivate the SC–S pathway in WT mice. **b**, Example coronal section (top) and magnified areas (bottom four) that contain the ZI and STN. The mCherry$^+$ cells in the ZI and STN are intermingled with EGFP$^+$ axon terminals from SC neurons. **c**, Example coronal section (top) and magnified area (bottom) showing EGFP$^+$ subthalamus-projecting SC neurons distributed in the intermediate layer and deep layer of the lateral SC. **d**, Merged and single-channel micrographs showing subthalamus-projecting SC neurons are dually labeled by mCherry and EGFP. **e**,**f**, Example behavioral ethograms (**e**) and quantitative analyses of hunting efficiency (**f**) of hungry mice with (TeNT) and without (Ctrl) selective inactivation of the SC–S pathway. **g**, Average time course of instantaneous locomotion speed of mice with (TeNT) and without (Ctrl) selective inactivation of the SC–S pathway in response to looming visual stimuli. Both groups of mice showed escape–freezing defensive behavior. Insets are heatmaps of the locomotion speed of example mice. **h**, Quantitative analyses of average speed before, during and after looming visual stimuli of mice with (TeNT) and without (Ctrl) selective inactivation of the SC–S pathway. **i**, Analyses of daily food intake of mice with (TeNT) and without (Ctrl) selective inactivation of the SC–S pathway. Morphological analyses (**a**–**d**) were independently repeated seven times with similar results obtained. Data in **f**–**i** are the mean ± s.e.m. (error bars), with the numbers of mice indicated in the graphs. The broken and unbroken red and white lines in the section images (**b**, **c**) represent boundaries of brain regions. Statistical analyses in **f**, **h** and **i** were performed using two-sided Student *t*-tests (***$P < 0.001$, **$P < 0.01$, NS, not significant ($P > 0.1$; applicable to all figures)).

these ChR2-mCherry$^+$ SC neurons (Fig. 3j). Photostimulation of ChR2-mCherry$^+$ axon terminals in the subthalamus (Fig. 3i) effectively promoted the efficiency of predatory hunting (Fig. 3k,l).

We also examined the role of subthalamus-projecting GABA$^+$ SC neurons in predatory hunting, even though the proportion of these cells is very small (Fig. 3d). AAV-DJ-EF1α-DIO-ChR2-mCherry was injected into the SC of *Gad2*-IRES-Cre mice, followed by optical fiber implantation above the subthalamus (Fig. 3g). The specific targeting of ChR2-mCherry to GABA$^+$ SC neurons was confirmed by immunohistochemistry and slice physiology analyses (Supplementary Fig. 11a–d). A light-pulse train (473 nm, 2 ms, 10 Hz, 20 mW) reliably evoked phase-locked spiking activity in these ChR2-mCherry$^+$ SC neurons (Supplementary Fig. 11e). ChR2-mCherry$^+$ axon terminals of SC GABA$^+$ neurons were too sparse to be detected in the subthalamus (Supplementary Fig. 11f). Photostimulation of these sparse ChR2-mCherry$^+$ axon terminals in the subthalamus did not promote the efficiency of hunting (Supplementary Fig. 11g). In fact, compared with glutamate$^+$ SC neurons, GABA$^+$ SC neurons labeled by ChR2-mCherry barely projected to major targets of the SC, suggesting that most of them may be interneurons (Supplementary Fig. 11h,i). These data indicate that glutamate$^+$ SC neurons, rather than GABA$^+$ SC neurons, constitute the key circuit module in the SC–S pathway that provokes predatory hunting.

Subthalamus-projecting SC neurons detect prey-derived visual and somatosensory cues. Next, we explored whether subthalamus-projecting SC neurons detect features of prey. We observed that mice strongly preferred to hunt a moving cockroach rather than a stationary one (Supplementary Video 9; Supplementary Fig. 12a,b), suggesting that motion of prey may be a key stimulus to trigger hunting. In different species, motion of prey can provide important salient sensory cues, for example, visual cues[1–3,6] and vibrissal somatosensory cues[5,21], for predators to distinguish prey from the background. Indeed, we found that either vibrissae trimming or darkness (~0.002 lux), which largely deprived vibrissal somatosensory or visual input, respectively, significantly impaired predatory hunting in mice (Fig. 4a,b). More importantly, simultaneous bimodal sensory deprivation exerted an additive effect that further reduced hunting efficiency (Figs. 4a,b), indicating that both vibrissal somatosensory and visual modalities participate in prey-capture behavior in mice.

These observations prompted us to test the hypothesis that subthalamus-projecting SC neurons are involved in detecting motion-related visual and vibrissal somatosensory cues of prey. To record the single-unit activity of subthalamus-projecting SC neurons, we employed an antidromic activation strategy[26]. AAV-DJ-EF1α-DIO-ChR2-mCherry was injected into the SC of *vGlut2*-IRES-Cre mice, followed by implantation of an optical fiber above the subthalamus. Three weeks after virus injection, single-unit recording was performed with a tungsten electrode in the SC of head-fixed awake mice. The putative subthalamus-projecting SC neurons were identified by the antidromic spikes evoked by light pulses (473 nm, 1 ms, 2 mW) illuminating ChR2-mCherry$^+$ axon terminals in the subthalamus (Fig. 4c). The antidromically evoked spikes had to conform to the following two criteria[27]: first, their latency to light pulse should be less than 5 ms, and second, their waveform should be similar to that of spikes evoked by sensory stimulation. With

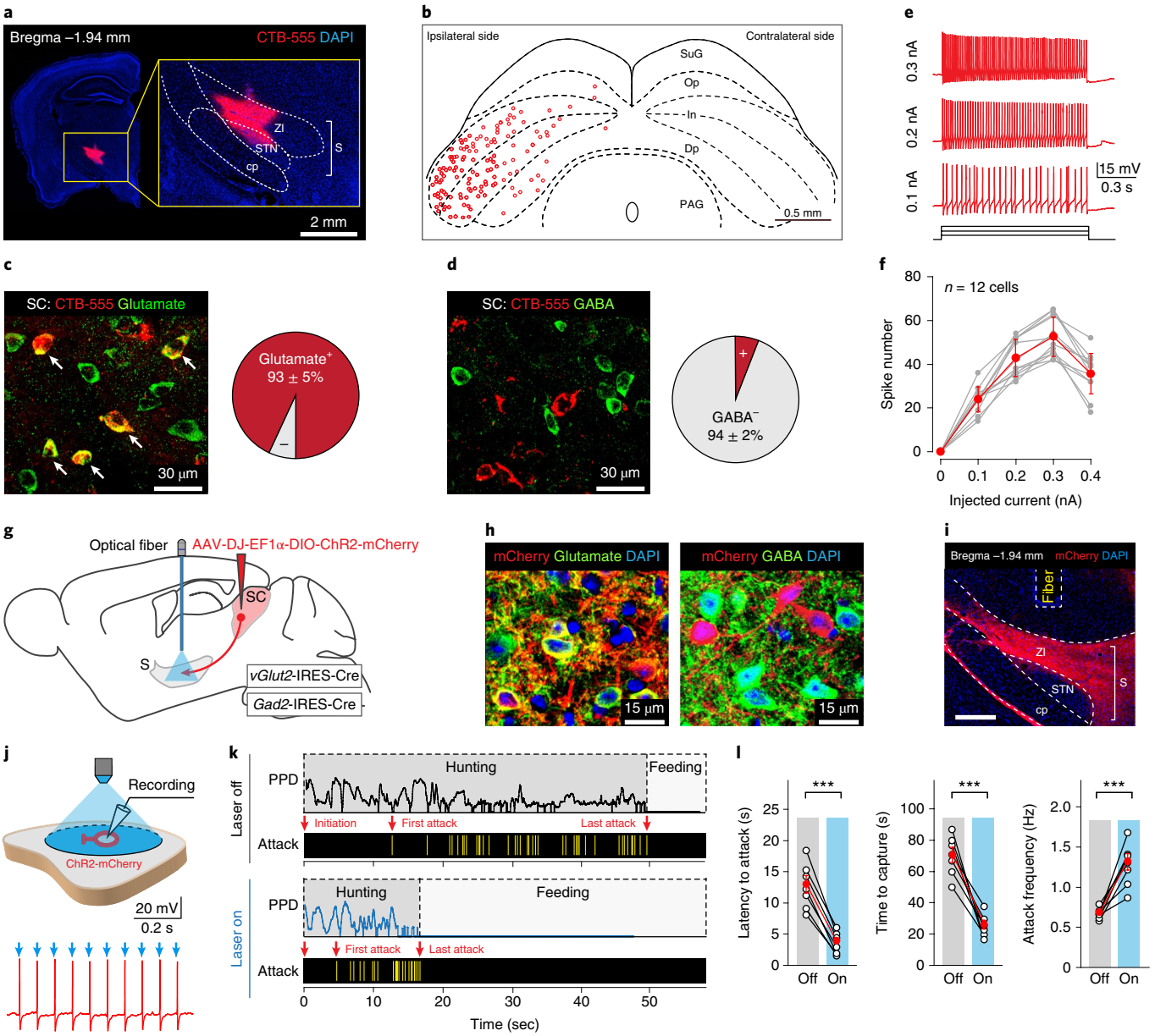

Fig. 3 | Characterization of subthalamus-projecting SC neurons. a, Example coronal section showing the unilateral injection of CTB-555 into the subthalamus. Inset: the injection center of CTB-555 was restricted within the ZI and STN, two major nuclei in the subthalamus. The experiment was independently repeated five times with similar results obtained. **b**, Schematic showing the distribution of CTB-555$^+$ cells in the SC (bregma -3.60 mm). **c**,**d**, Example micrographs (left) and quantitative analyses (right) showing CTB-555$^+$ cells in the SC are predominantly positive for glutamate (**c**) and negative for GABA (**d**). Arrows in **c** indicate cells double-positive for CTB-555 and glutamate. Results are from $n = 5$ mice. **e**, Example traces of AP spiking activity evoked by depolarizing currents injected into EGFP$^+$ subthalamus-projecting SC neurons. **f**, Quantitative analyses of spike number as a function of current intensity. **g**, Schematic showing injection of AAV-DJ-EF1α-DIO-ChR2-mCherry into the SC of *vGlut2*-IRES-Cre or *Gad2*-IRES-Cre mice, followed by ipsilateral optical fiber implantation above the subthalamus to enable cell-type-specific activation of the SC–S pathway. **h**, Example micrographs from the SC intermediate layer showing cell-type-specific expression of ChR2-mCherry in glutamate$^+$ (left) and GABA$^+$ neurons (right) in *vGlut2*-IRES-Cre mice. The experiment was independently repeated five times with similar results obtained. **i**, Example coronal section from *vGlut2*-IRES-Cre mice, showing the track of the optical fiber implanted above the subthalamus, where ChR2-mCherry$^+$ axon terminals were optogenetically stimulated. The experiment was independently repeated in 7 mice with similar results obtained. Scale bar, 0.4 mm. **j**, Example traces of phase-locked spiking activity evoked by a light-pulse train (10 Hz, 2 ms, 20 mW) from ChR2-mCherry$^+$ neurons in acute SC slices of *vGlut2*-IRES-Cre mice. **k**,**l**, Example behavioral ethograms (**k**) and quantitative analyses (**l**) of latency to attack, time to capture and attack frequency of mice with (On) or without (Off) optogenetic activation of the glutamate$^+$ SC–S pathway ($n = 7$ mice). The broken white lines in the section images (**a**, **b**, **i**) represent boundary of brain regions. The red lines in **l** represent averaged data. Data in **c**, **d**, **f** and **l** are the mean ± s.e.m. Statistical analyses in **l** were performed using two-sided Student *t*-tests (***$P < 0.001$).

these criteria, we identified 21 putative subthalamus-projecting SC neurons, which exhibited low spontaneous firing (0.16 ± 0.03 Hz, $n = 21$ units). With short latencies to light pulses (2.7 ± 0.4 ms, $n = 21$ units; Fig. 4d), the antidromically evoked spikes possessed waveforms quantitatively correlated with those evoked by sensory stimulation (Fig. 4e).

Next, we examined the single-unit responses of subthalamus-projecting SC neurons to prey-derived sensory cues. To simulate

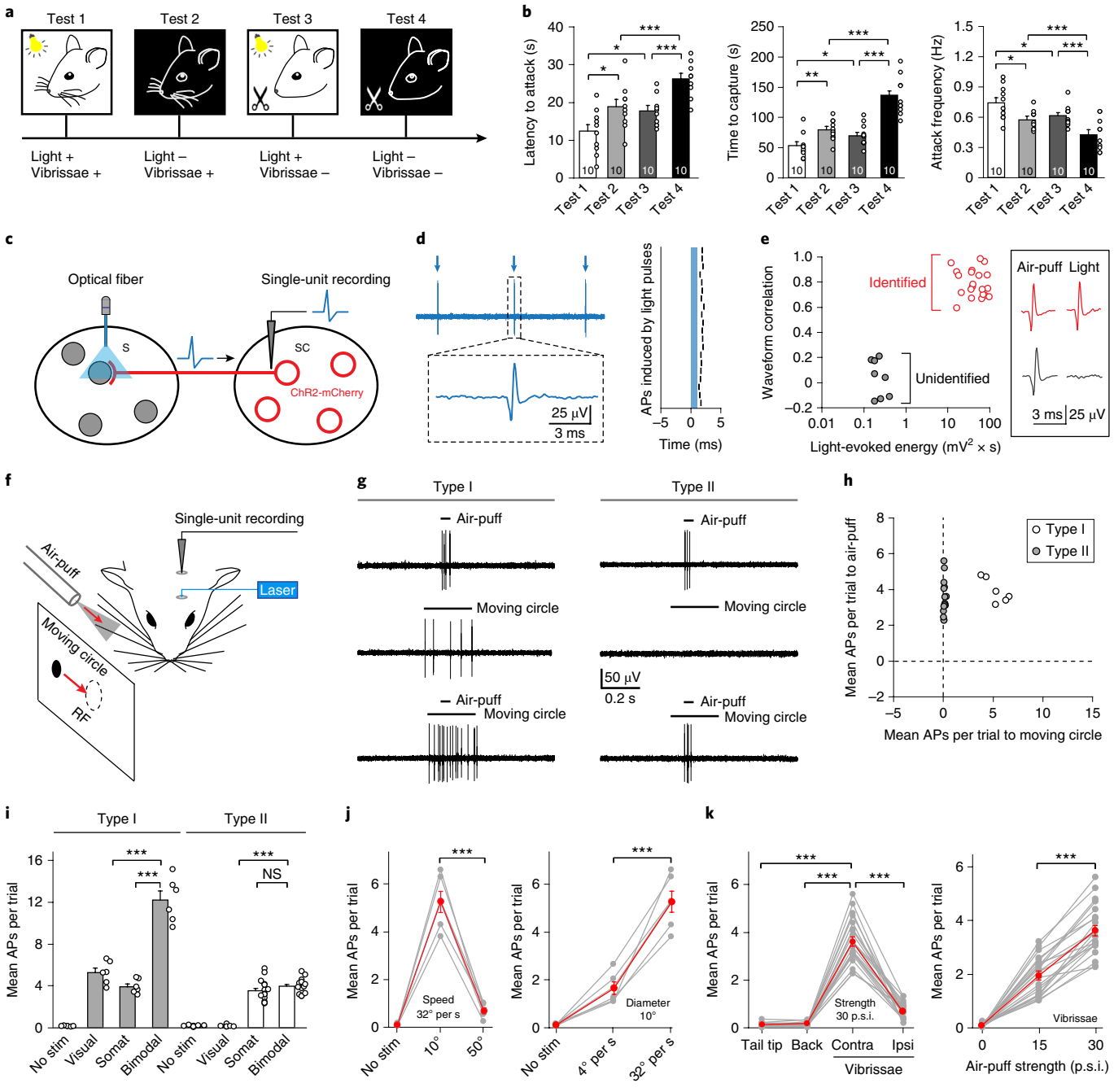

Fig. 4 | Single-unit recording from antidromically identified subthalamus-projecting SC neurons. a, Schematic of the procedure for testing hunting efficiency after sequential deprivation of visual or vibrissal somatosensory inputs. **b**, Quantitative analyses of hunting efficiency of mice subjected to sequential visual and vibrissal sensory deprivation. **c**, Schematic of the antidromic activation strategy for identifying the single-unit activity of subthalamus-projecting SC neurons. **d**, An example trace of light-evoked action potentials (APs) (left) and the analyses of latency (right) showing the identification of subthalamus-projecting SC neurons. **e**, Correlation analysis of APs evoked by light pulse and by vibrissal air-puff of individual units, confirming a segregation between antidromically identified units (red circles and traces) and non-identified units (gray circles and traces). The waveform correlation was calculated as cross-correlation coefficients between spontaneous and light-evoked spike waveforms with a lag of 0 ms. **f**, Schematic showing the visual stimulation (a black circle moving across the receptive field (RF) on a tangent screen, temporal to nasal) and vibrissal somatosensory stimulation (air-puff, temporal to nasal). **g**, Example traces of a type I unit and a type II unit to vibrissal somatosensory stimulus alone (top row, 30 p.s.i., 50 ms), visual stimulus alone (middle row, 10°, 32° per s), and bimodal sensory stimuli (bottom row). **h**, Distribution of responses to visual and vibrissal somatosensory stimuli of all the identified subthalamus-projecting SC units. **i**, Quantitative analyses of sensory responses of type I ($n = 6$) and type II units ($n = 15$) to no stimulus (No stim) visual stimulus alone (Visual), vibrissal somatosensory stimulus alone (Somat) and bimodal sensory stimuli (Bimodal), showing the additive effect of bimodal stimuli on the evoked response of type I units. **j**, Quantitative analyses of visual responses of type 1 units ($n = 6$) to a moving black circle of different diameters and at different speeds. **k**, Quantitative analyses of somatosensory responses of type I and II units ($n = 21$) to air-puffs (50 ms) directed toward different body parts and with different strengths. Red lines in **j** and **k** represent averaged data. Data in **b**, **i**, **j** and **k** are the mean ± s.e.m. Statistical analyses in **b**, **i**, **j** and **k** were performed using two-sided Student *t*-tests (***$P < 0.001$, **$P < 0.01$, *$P < 0.05$).

the visual cues of moving prey, a computer-generated black circle (diameter of 10°) moving at a controlled velocity (32° per s) and direction (temporal-to-nasal) was projected onto a tangent screen (Fig. 4f; Supplementary Fig. 13a). To mimic the somatosensory cues of moving prey, brief gentle air-puffs (50 ms, 30 p.s.i.) generated by a Picospritzer were delivered to vibrissae (temporal-to-nasal) of head-fixed awake mice[19] (Fig. 4f). We quantified their responses to these prey-like sensory stimuli by measuring the number of spikes per trial[17]. According to their responses to visual and somatosensory stimuli, the 21 single units were quantitatively categorized into two types. Type I units (6 out of 21) responded to both visual and vibrissal somatosensory stimuli, whereas type II units (15 out of 21) responded only to somatosensory stimuli (Fig. 4g,h). Importantly, simultaneous bimodal sensory stimuli evoked additive responses from type I units (Fig. 4g,i), suggesting that there is a multisensory integration mechanism in these functional units.

To better describe the sensory response properties of subthalamus-projecting SC neurons, we separately analyzed their responses to visual and vibrissal somatosensory stimuli. The visual responses of these neurons (type I units, $n=6$) preferred a small circle (10° compared with 50°) moving at high speed (32° per s compared with 4° per s) (Fig. 4j). The visual receptive fields were clustered within the nasal and ventral quadrant of the mouse visual field (Supplementary Fig. 13b). The subthalamus-projecting SC neurons (type I and II units, $n=21$) responded predominantly to air-puffs directed toward the vibrissal region contralateral to the recorded side (Fig. 4k; Supplementary Fig. 13c). Their responses adapted faster to repetitive vibrissal somatosensory stimuli with higher frequency (2 Hz compared with 0.5 Hz; Supplementary Fig. 13d). The averaged peristimulus time histograms of type I and type II units were also analyzed (Supplementary Fig. 13e,f). The sites of single-unit recording were all located within the intermediate layer of the lateral SC (Supplementary Fig. 13g,h).

Subthalamus-projecting SC neurons transform sensory cues into attack-related neural signals. How do subthalamus-projecting SC neurons translate prey-derived sensory cues into neural signals of predatory hunting in real-time? To address this question, we recorded GCaMP signals from subthalamus-projecting SC neurons[28,29]. AAV2-retro-EF1α-DIO-GCaMP6s was injected into the subthalamus of *vGlut2*-IRES-Cre mice, followed by implantation of an optical fiber above the subthalamus-projecting SC neurons in the intermediate layer of the lateral SC (Fig. 5a). This strategy resulted in the expression of GCaMP6s specifically in glutamate$^+$ SC neurons (Fig. 5b; Supplementary Fig. 14a,b). The reliability of AAV2-retro-EF1α-DIO-GCaMP6s to retrogradely label subthalamus-projecting SC neurons was further verified in a control experiment (Supplementary Fig. 14c–e).

Then, we recorded GCaMP signals of subthalamus-projecting SC neurons in freely moving mice during predatory hunting. We observed a strong transient increase in GCaMP fluorescence when mice attacked prey with their jaws (Fig. 5c; Supplementary Video 10). By contrast, GCaMP fluorescence only mildly increased in the control experiment, in which mice investigated a three-dimensional (3D) object (wooden cube) (Fig. 5d; Supplementary Video 11). The normalized GCaMP fluorescence change ($\Delta F/F$) during predatory hunting was significantly higher than that during investigation of the object (Fig. 5e). We did not observe fluorescence changes from SC neurons expressing EGFP during predatory hunting, indicating that the recorded signals were not motion artifacts (Supplementary Fig. 15a,b).

During predatory hunting, mice exhibit a stereotypical sequence of actions (approaching, attacking and consuming prey) that are triggered by prey-derived sensory cues[6]. To further determine when the activity of subthalamus-projecting SC neurons are activated relative to the entire action sequence of hunting, we performed fiber photometry recording in mice hunting for a live cockroach restrained in a corner of an arena (Supplementary Fig. 15c). In this paradigm, the predator approached and then attacked the restrained prey (Supplementary Video 12). We found that subthalamus-projecting SC neurons were not activated in the phase of approach. By contrast, strong GCaMP fluorescence was elicited when the predator began to attack the prey (Supplementary Fig. 15d,e). These data indicate that subthalamus-projecting SC neurons are specifically activated during predatory attack.

To further examine the temporal relationship between GCaMP signals and predatory attack, we aligned the GCaMP signals to the initiation of individual attacks (Fig. 5f). We defined the onset time of the GCaMP signal as the time when the signal reached 15% of the peak amplitude relative to the baseline. The average GCaMP signal started to rise at 118 ± 21 ms before the initiation of jaw attacks ($n=5$ mice; Fig. 5g).

To examine whether the attack-associated activity of subthalamus-projecting SC neurons depended on sensory inputs, we recorded GCaMP signals in hunting mice subjected to sensory deprivation. We found that either vibrissae trimming or darkness in the arena delayed the onset time and reduced the amplitude of attack-associated GCaMP signals (Fig. 5g–k). More importantly, simultaneous vibrissae trimming and darkness in the arena exerted an additive effect that strongly reduced the amplitude of GCaMP signals (Fig. 5j,k). Thus, the sensory-dependent GCaMP signals suggest that subthalamus-projecting SC neurons may transform prey-derived sensory cues into neural signals for predatory attack.

The ZI mediates predatory hunting provoked by SC–S pathway activation. We next explored the postsynaptic target nuclei in the subthalamus that mediate the behavioral effects of SC–S pathway activation. In the subthalamus, the ZI and STN, but not other nuclei, receive synaptic inputs from the SC[30–32]. We injected AAV-DJ-hSyn-ChR2-mCherry into the SC of WT mice, resulting in labeling of ChR2-mCherry$^+$ axons predominantly in the ZI rather than the STN (Fig. 6a,b; also see Figs. 1h and 3i). These morphological observations were further supported by slice physiology analyses (Fig. 6c–e). In acute brain slices of the subthalamus (Fig. 6c), light pulses (473 nm, 2 ms, 20 mW) illuminating ChR2-mCherry$^+$ axon terminals from the SC evoked robust postsynaptic currents (PSCs) from ZI neurons (219 ± 27 pA, $n=8$ neurons), whereas the same light stimulation program evoked weak PSCs from STN neurons (24 ± 2 pA, $n=8$ neurons; Fig. 6d). The light-evoked PSCs from ZI neurons were mediated by glutamate receptors (Fig. 6e). Thus, the ZI is a major postsynaptic target of the SC–S pathway.

To examine whether the ZI or STN mediates predatory hunting provoked by SC–S pathway activation, we first assessed the cell-type specificity of these two nuclei. Consistent with previous studies[33,34], we found that a large proportion of ZI neurons are GABAergic, whereas the majority of STN neurons are glutamatergic (Supplementary Fig. 16a–c). In WT mice (Supplementary Fig. 16d–k), $86\pm2.6\%$ of ZI neurons were GABA$^+$ ($n=5$ mice), whereas $95\pm1.2\%$ STN neurons were predominantly glutamate$^+$ ($n=5$ mice). The dichotomy of cell-type specificity in the ZI and STN provided an opportunity to selectively inactivate one of these nuclei using genetic approaches.

To examine whether the ZI mediates predatory hunting provoked by SC–S pathway activation, a two-step viral injection procedure was used (Fig. 6f). First, AAV-DJ-EF1α-DIO-EGFP-2A-TeNT was bilaterally injected into the subthalamus of *Gad2*-IRES-Cre mice, with AAV-DJ-EF1α-DIO-EGFP as a control. Second, AAV-DJ-hSyn-ChR2-mCherry was bilaterally injected into the SC, followed by implantation of an optical fiber above the bilateral subthalamus. This strategy resulted in the expression of EGFP and TeNT in ZI neurons that were intermingled with ChR2-mCherry$^+$

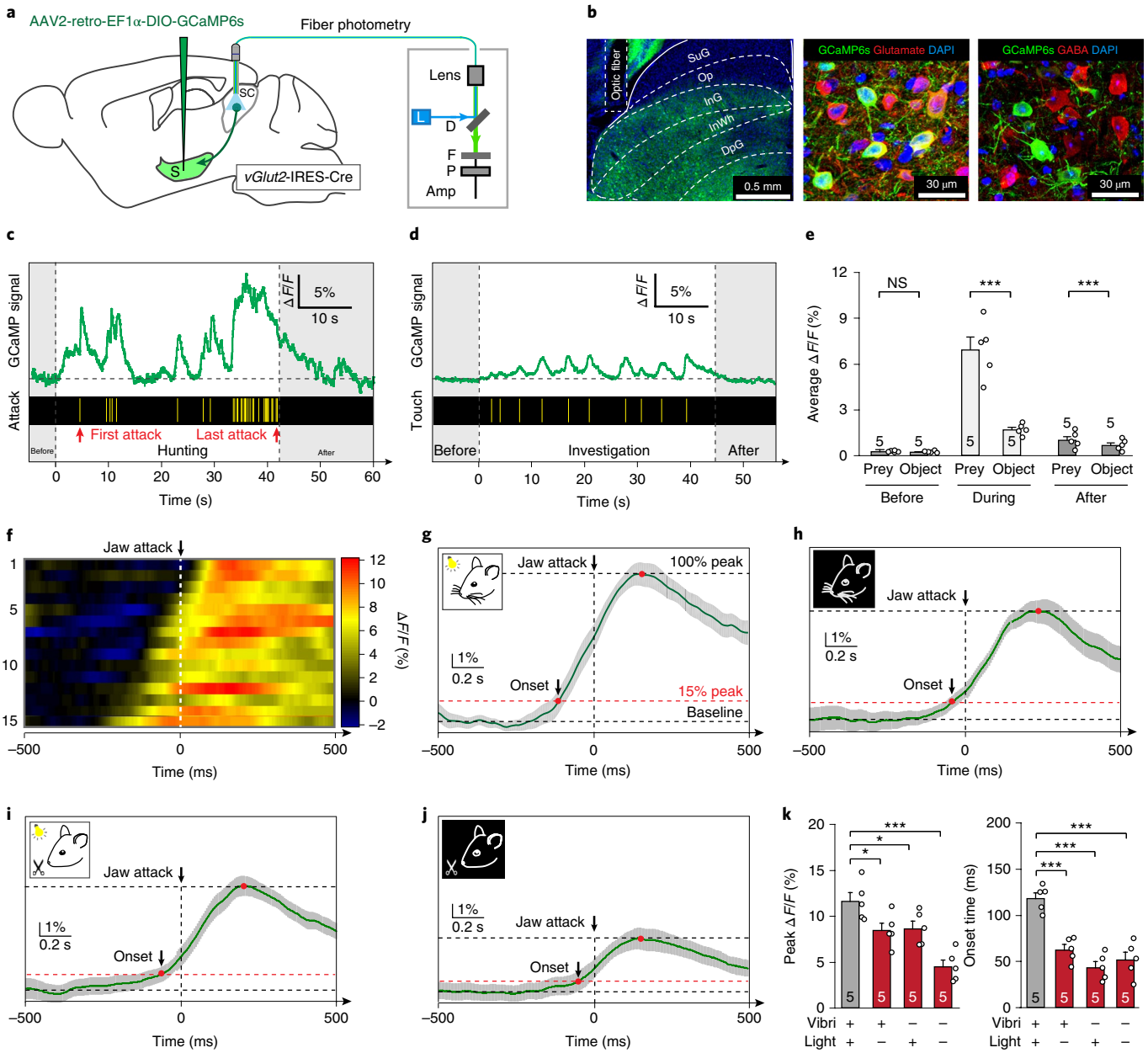

Fig. 5 | Subthalamus-projecting SC neurons specifically encode predatory attack. a, Schematic of the injection of AAV2-retro-EF1α-DIO-GCaMP6s into the subthalamus of *vGlut2*-IRES-*Cre* mice, followed by optical fiber implantation above the SC for fiber photometry recording. L, laser; D, dichroic mirror; F, filter; P, photomultiplier tube; Amp, amplifier. **b**, Example micrographs showing the optical fiber track above the GCaMP$^+$ SC neurons (left), which were immunohistochemically verified to be positive for glutamate (middle) and negative for GABA (right). The experiment was independently repeated with similar results in $n = 5$ mice. The broken and unbroken lines in the image represent boundaries of brain regions. **c**, GCaMP signal in parallel with jaw attacks during predatory hunting in an example mouse. See Supplementary Video 9 for details. **d**, GCaMP signal in parallel with vibrissal investigation of a textured object in an example mouse. See Supplementary Video 10 for details. **e**, Quantitative analyses of average GCaMP fluorescence change ($\Delta F/F$) before, during and after hunting for prey (Prey) or investigating a textured object (Object). **f**,**g**, Heatmap of individual GCaMP signals (**f**) and an averaged GCaMP response curve (**g**) aligned with the initiation of jaw attacks, showing the kinetics of GCaMP signals from subthalamus-projecting SC neurons. **h**–**j**, Averaged GCaMP response curves aligned with the initiation of jaw attacks of mice subjected to deprivation of visual input alone (**h**), vibrissal somatosensory input alone (**i**) or bimodal sensory inputs (**j**). **k**, Quantitative analyses of amplitude and onset time of GCaMP signals from mice with and without sensory (light and/or vibrissal (Vibri)) deprivation. Data in **e** and **k** are the mean ± s.e.m (error bars). The curves and shaded regions in **g**–**j** indicate the mean ± s.e.m. Numbers of mice are indicated in the graphs (**e** and **k**). Statistic analyses in **e** and **k** were performed using two-sided Student's *t*-tests (***$P < 0.001$, *$P < 0.05$).

axon terminals from SC neurons (Fig. 6g, left). As a control experiment, we found that expression of TeNT in ZI neurons did not alter neurotransmitter release from subthalamus-projecting SC neurons (Supplementary Fig. 17). The ZI neurons expressing EGFP and TeNT were confirmed to be GABA$^+$ (Supplementary Fig. 18a). We found that TeNT-mediated synaptic inactivation of GABA$^+$ ZI neurons significantly impaired the basal level of predatory hunting (Supplementary Fig. 18b). More importantly, this manipulation almost completely abrogated the increased hunting efficiency induced by optogenetic activation of the SC–S pathway (Fig. 6h).

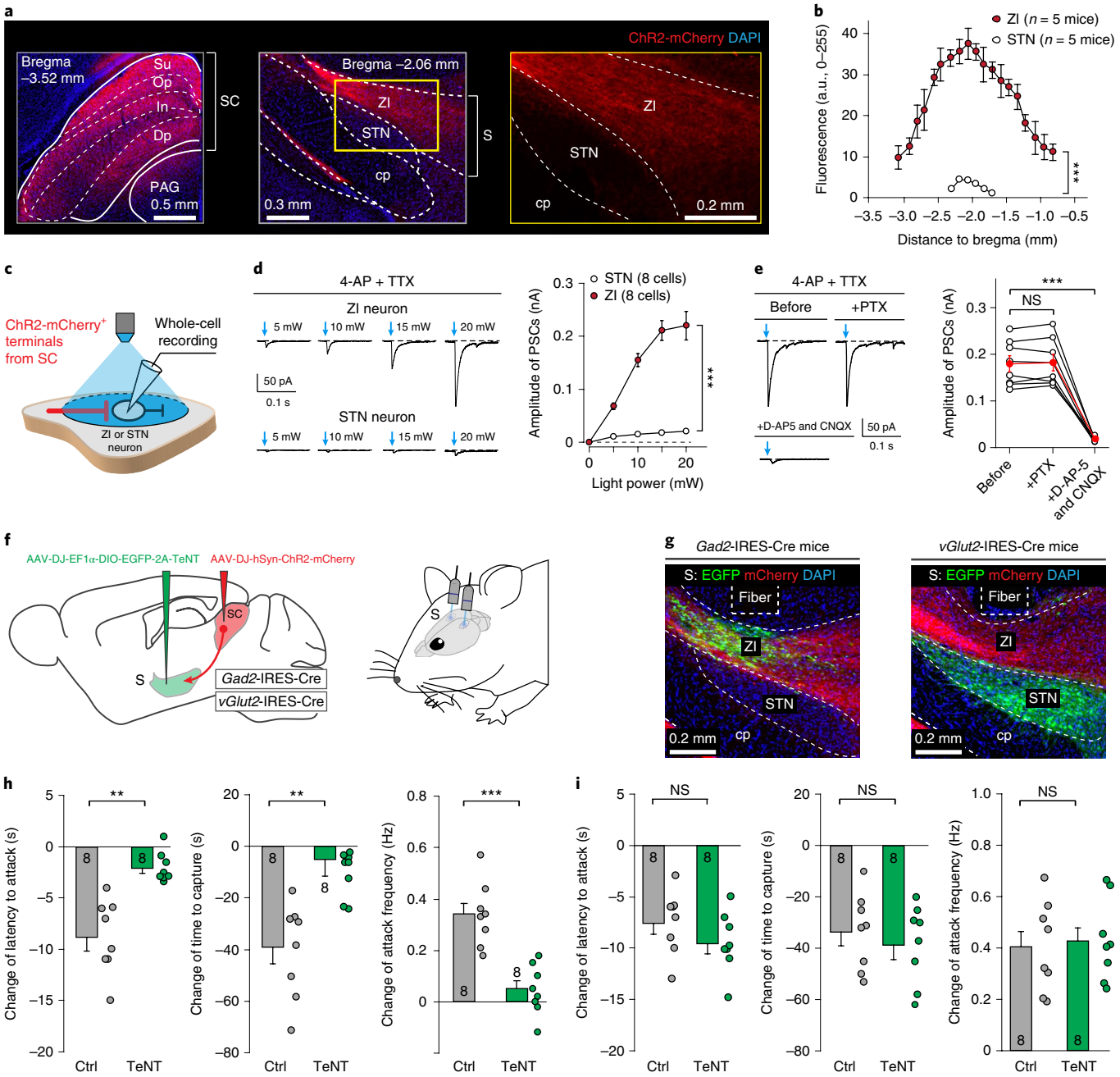

Fig. 6 | GABA⁺ ZI neurons are the postsynaptic target of the SC–S pathway to mediate sensory-triggered predatory hunting. a, AAV-DJ-hSyn-ChR2-mCherry was injected into the SC of WT mice (left), resulting in ChR2-mCherry⁺ axons distributed predominantly in the ZI but not in the STN (middle and right). **b**, Quantitative analyses of mCherry fluorescence in the ZI and STN as a function of the distance to bregma. **c**, Schematic showing the recording of PSCs from ZI or STN neurons evoked by photostimulation of ChR2-mCherry⁺ axon terminals in the subthalamus of acute brain slices. **d**, Example traces (left) and quantitative analyses (right) of the amplitude of light-evoked PSCs (in the presence of 4-AP and TTX) recorded from STN and ZI neurons. **e**, Example traces (left) and quantitative analyses (right) showing the effects of antagonists of $GABA_A$ receptors (picrotoxin; PTX) and glutamate receptors (D-AP5 and CNQX) on light-evoked PSCs recorded from ZI neurons. **f**, Schematic showing AAV-DJ-EF1α-DIO-EGFP-2A-TeNT and AAV-DJ-hSyn-ChR2-mCherry injection into the subthalamus and SC of *vGlut2*-IRES-Cre or *Gad2*-IRES-Cre mice (left), followed by optical fiber implantation above the subthalamus (right). **g**, Example micrographs showing EGFP⁺ ZI (left) or STN neurons (right) intermingled with ChR2-mCherry⁺ axon terminals from the SC. The experiment was independently repeated eight times with similar results obtained. **h**, TeNT-mediated synaptic inactivation of GABA⁺ ZI neurons significantly attenuated the effects of optogenetic activation of the SC–S pathway on hunting efficiency. **i**, TeNT-mediated synaptic inactivation of glutamate⁺ STN neurons did not significantly attenuate the effects of optogenetic activation of the SC–S pathway on hunting efficiency. Data in **b**, **d**, **h** and **i** are the mean ± s.e.m. (error bars). The broken and unbroken lines in **a** and **g** represent boundaries of brain regions. The numbers of cells (**d**) and mice (**h** and **i**) are indicated in the graphs. Statistical analyses in **e**, **h** and **i** were performed using two-sided Student's t-tests (**$P < 0.01$, ***$P < 0.001$). Statistical analyses in **b** and **d** were performed using one-way analysis of variance (***$P < 0.001$).

To examine whether the STN mediates predatory hunting provoked by SC–S pathway activation, we injected AAV-hSyn-ChR2-mCherry and AAV-EF1α-DIO-EGFP-2A-TeNT bilaterally into the SC and subthalamus, respectively of *vGlut2*-IRES-Cre mice, followed by optical fiber implantation above the subthalamus (Fig. 6f). This strategy resulted in the expression of EGFP and TeNT specifically in the STN neurons (Fig. 6g, right). The STN neurons expressing EGFP were positive for glutamate (Supplementary Fig. 18c). TeNT-mediated synaptic inactivation of glutamate$^+$ STN neurons did not attenuate either the efficiency of basal predatory hunting (Supplementary Fig. 18d) or the behavioral effects of SC–S pathway activation (Fig. 6i). Together, these data suggest that the ZI, but not the STN, mediates predatory hunting provoked by SC–S pathway activation.

GABA$^+$ ZI neurons are both necessary and sufficient for predatory hunting. Next, we explored the role of GABA$^+$ ZI neurons in predatory hunting via light-mediated local and acute inhibition of GABA$^+$ ZI neurons. AAV-DJ-EF1α-DIO-GtACR1-EGFP[35] was bilaterally injected into the subthalamus of *Gad2*-IRES-Cre mice, followed by implantation of an optical fiber above the ZI (Supplementary Fig. 19a,b). Light illumination (473 nm, 500 ms, 20 mW) on acute slices effectively prevented the spiking activity of GtACR-EGFP$^+$ ZI neurons (Supplementary Fig. 19c). Photoinhibition of GABA$^+$ ZI neurons bilaterally (473 nm, 15 s on and 15 s off, 20 mW) via GtACR1 strongly decreased hunting efficiency (Supplementary Fig. 19d), without altering the object-exploration behavior in mice (Supplementary Fig. 19e).

We also examined whether unilateral inactivation of GABA$^+$ ZI neurons affected predatory hunting. In a T-shaped arena with one corridor interconnected to two chambers, a predator was allowed to go through the corridor and freely hunt for restrained prey in both chambers (Supplementary Fig. 20a). In the control experiment, the intact WT mice hunted for prey with balanced probabilities ($P_{Left} = 0.52 \pm 0.03$, $P_{Right} = 0.48 \pm 0.03$) and similar hunting efficiency (Supplementary Fig. 20b). Mice with unilateral inactivation of GABA$^+$ ZI neurons (Supplementary Fig. 20c) preferred prey on the ipsilateral side of inactivation ($P_{Ipsilateral} = 0.58 \pm 0.03$, $P_{Contralateral} = 0.42 \pm 0.03$). Similarly, mice with unilateral inactivation of glutamate$^+$ SC neurons (Supplementary Fig. 20e) exhibited preference for prey ipsilateral to the inactivated SC ($P_{Ipsilateral} = 0.72 \pm 0.04$, $P_{Contralateral} = 0.28 \pm 0.04$). However, the hunting efficiency for ipsilateral or contralateral prey was not significantly altered by unilateral inactivation of GABA$^+$ ZI neurons (Supplementary Fig. 20d) or unilateral inactivation of the SC (Supplementary Fig. 20f). These data suggest that in mice with unilateral inactivation of the ZI or SC, the intact side could partially compensate for the function of the inactivated side.

Finally, we examined whether activation of GABA$^+$ ZI neurons is sufficient to promote hunting efficiency. AAV-DJ-EF1α-DIO-ChR2-mCherry was injected into the subthalamus of *Gad2*-IRES-Cre mice, followed by implantation of an optical fiber above the ZI (Supplementary Fig. 21a,b). In acute slices of the ZI, a light-pulse train (473 nm, 2 ms, 10 Hz, 20 mW) reliably triggered phase-locked spiking activity from the ChR2-mCherry$^+$ ZI neurons (Supplementary Fig. 21c). In vivo photostimulation of ZI GABA$^+$ neurons strongly promoted the efficiency of predatory hunting, without altering the object-exploration behavior in mice (Supplementary Fig. 21d,e). These data indicate that ZI GABA$^+$ neurons are sufficient to trigger predatory hunting. A recent study reported that GABA$^+$ ZI neurons encode a positive motivational valence[36], raising the possibility that activation of ZI GABA$^+$ neurons can motivate mice to hunt for prey. To test this hypothesis, we initiated an independent study, which is described in the accompanying manuscript[37].

The SC–MLR pathway may participate in guiding the mouse to the prey. How is the predator guided to the prey during hunting? Among the tectofugal pathways labeled in FosTRAP mice (Supplementary Fig. 4e), we noted the pathway projecting to the mesencephalic locomotor region (MLR), which consists of the pedunculopontine tegmental nucleus (PPTg) and cuneiform nucleus (CnF). The SC neurons projecting to the MLR were broadly distributed in the intermediate and deep layers of the SC and rarely sent collaterals to the subthalamus (Supplementary Fig. 22). As the MLR has been implicated in the initiation and termination of mouse locomotion[38,39], we hypothesized that the SC–MLR pathway may participate in guiding the predator to the prey.

We tested this hypothesis via three experiments. First, we found that the GCaMP signals of MLR-projecting SC neurons increased when the predator started to approach the prey (Supplementary Video 13; Supplementary Fig. 23a–c). The approach/attack ratio of GCaMP signals of the SC–MLR pathway was significantly higher than that of the SC–S pathway (Supplementary Fig. 23d,e), supporting the notion that the SC–MLR pathway is probably involved in prey approach. Second, SC–MLR pathway activation evoked locomotion (Supplementary Fig. 24). Third, bilateral inactivation of this pathway reduced locomotion speed during predatory hunting, which was not observed in mice with SC–S pathway inactivation (Supplementary Fig. 25). Together, these three lines of evidence suggest that the SC–MLR pathway is probably involved in guiding the mouse to the prey during predatory hunting.

Discussion

Predatory hunting is an evolutionarily conserved behavior that is triggered by prey-derived sensory cues. In mammalian brains, the specific circuits that convert prey-derived sensory cues into prey-capture behavior have yet not been reported. Here, we identified a subset of SC neurons that are sufficient and necessary for predatory hunting in mice (Figs. 1–3). These neurons respond to motion-related visual and somatosensory cues from prey (Fig. 4). During hunting, they send motor signals to the ZI to trigger predatory attack (Figs. 5 and 6). Together, these data revealed how the brain transforms prey-derived sensory cues into predatory attack during hunting behavior in mice.

Prey-derived features trigger prey-capture behavior in mice. In different species[1–6], it is the feature of prey that triggers prey-capture behavior. In Ewert's classical experiment[1], a black bar moving in a direction parallel to its long axis (worm-like configuration) triggered prey-capture behavior in toads. The same bar oriented perpendicularly to the moving direction (anti-worm configuration) was ignored by toads. These observations argued that a bar with a worm-like configuration is the key stimulus to trigger prey-capture behavior in toads[1]. We found that mice strongly preferred to hunt a moving cockroach rather than a stationary one, suggesting that motion of prey may be a key stimulus for hunting in mice. In different species, motion of prey provides biologically salient cues, for example visual cues[1–3,6] and somatosensory cues[5,21], for predators to distinguish prey from the background.

Subthalamus-projecting SC neurons detect the features of prey. How do mice detect motion of prey? The subthalamus-projecting SC neurons, which optimally respond to a small moving visual target and/or air-puffs at the vibrissal area, may be an important substrate for detecting motion of prey. Interestingly, type I units detect multiple sensory cues of prey. The somatosensory responses may originate from the trigeminal complex and the primary somatosensory cortex in rodents[40]. The visual responses may be relayed by inter-laminar projections from retina-recipient layers to the intermediate layer of the SC[16]. Together with the classical work on multisensory integration in cats and monkeys[41,42], our

observation suggests that multisensory integration is conserved in rodents and is critical for sensory-triggered behavior such as predatory hunting.

Functional analyses of the SC–S pathway revealed its causal role in sensory-triggered predatory hunting. TeNT-mediated synaptic inactivation of the SC–S pathway impaired processing of both visual and vibrissal somatosensory information, consequently preventing predatory hunting in mice. Conversely, photostimulation of the SC–S pathway, which encodes specific prey features, was sufficient to release the behavioral program of predatory hunting.

The SC–S pathway may specifically participate in predatory hunting. The specific role of the SC–S pathway in predatory hunting was supported by three lines of evidence. First, SC–S pathway activation did not induce food intake, social aggression or exploration of a 3D object. Second, inactivation of the SC–S pathway did not alter visually triggered escape behavior, daily food intake or exploration of a 3D object. Third, the activity of the SC–S pathway during predatory attack was fourfold stronger than that for exploration of a 3D object. We noted that SC–S pathway activation triggered hunting-like actions to bedding material in the absence of prey. However, these actions may not be interpreted as an engagement with 3D objects, because neither activation nor inactivation of this pathway altered exploratory behavior toward the 3D object.

The SC–S pathway may link sensory processing to hunting motivation. We demonstrated that GABA$^+$ ZI neurons are postsynaptic targets of the SC–S pathway to provoke prey capture. These results and a recent report[36] indicating that ZI GABA$^+$ neurons encode positive motivational valence suggest that the SC–ZI pathway may link sensory processing to hunting motivation. This hypothesis was tested and the results are described in the accompanying paper[37]. In addition, GABA$^+$ ZI neurons may participate in somatosensory processing[43,44] and sleep regulation[45].

Recent studies have demonstrated that specific neuronal populations in the central amygdala, the lateral hypothalamus and the medial preoptic area participate in predatory hunting in mice[24,29,46]. The ZI directly or indirectly project to these interconnected limbic structures[47]. Therefore, our results suggest that the SC, as a brain region for sensory processing[9,10] and sensorimotor transformation[11], may provide a prey-relevant neural signal to these interconnected limbic structures en route to the ZI.

New questions. Our results raise several new questions. First, we monitored the population activity of subthalamus-projecting SC neurons in hunting mice. In future studies, it would be crucial to employ a miniaturized microscope to monitor their activity at the single-cell level[48]. Second, how is the mouse guided to the prey during prey capture? Our data suggest that the SC–MLR pathway may participate in this process. However, the detailed mechanisms remain to be elucidated. Finally, it is challenging to propose a computational model to understand how the brain rapidly recognizes prey according to the feature of target motion. Recent progress in information science may provide important insights into this question[49,50]. A previous study[49] has established biologically inspired computational models for recognizing visual targets. Continued promising efforts in this direction may address these questions.

Online content

Any methods, additional references, Nature Research reporting summaries, source data, statements of data availability and associated accession codes are available at https://doi.org/10.1038/s41593-019-0405-4.

Received: 18 November 2018; Accepted: 6 March 2019;
Published online: 24 May 2019

References

1. Ewert, J. P. Neural correlates of key stimulus and releasing mechanism: a case study and two concepts. *Trends Neurosci.* **20**, 332–339 (1997).
2. Gahtan, E., Tanger, P. & Baier, H. Visual prey capture in larval zebrafish is controlled by identified reticulospinal neurons downstream of the tectum. *J. Neurosci.* **25**, 9294–9303 (2005).
3. Bianco, I. H. & Engert, F. Visuomotor transformations underlying hunting behavior in zebrafish. *Curr. Biol.* **25**, 831–846 (2015).
4. Butler, K. Predatory behavior in laboratory mice: strain and sex comparisons. *J. Comp. Physiol. Psychol.* **85**, 243–249 (1973).
5. Anjum, F., Turni, H., Mulder, P. G., van der Burg, J. & Brecht, M. Tactile guidance of prey capture in etruscan shrews. *Proc. Natl Acad. Sci. USA* **103**, 16544–16549 (2006).
6. Hoy, J. L., Yavorska, I., Wehr, M. & Niell, C. M. Vision drives accurate approach behavior during prey capture in laboratory mice. *Curr. Biol.* **26**, 3046–3052 (2016).
7. Kim, C. K., Adhikari, A. & Deisseroth, K. Integration of optogenetics with complementary methodologies in systems neuroscience. *Nat. Rev. Neurosci.* **18**, 222–235 (2017).
8. Luo, L., Callaway, E. M. & Svoboda, K. Genetic dissection of neural circuits: a decade of progress. *Neuron* **98**, 256–281 (2018).
9. Seabrook, T. A., Burbridge, T. J., Crair, M. C. & Huberman, A. D. Architecture, function, and assembly of the mouse visual system. *Annu. Rev. Neurosci.* **40**, 499–538 (2017).
10. Cang, J., Savier, E., Barchini, J. & Liu, X. Visual function, organization, and development of the mouse superior colliculus. *Annu. Rev. Vis. Sci.* **4**, 239–262 (2018).
11. Gandhi, N. J. & Katnani, H. A. Motor functions of the superior colliculus. *Annu. Rev. Neurosci.* **34**, 205–231 (2011).
12. Basso, M. A. & May, P. J. Circuits for action and cognition: a view from the superior colliculus. *Annu. Rev. Vis. Sci.* **3**, 197–226 (2017).
13. Wang, L., Sarnaik, R., Rangarajan, K., Liu, X. & Cang, J. Visual receptive field properties of neurons in the superficial superior colliculus of the mouse. *J. Neurosci.* **30**, 16573–16584 (2010).
14. Hong, Y. K., Kim, I. J. & Sanes, J. R. Stereotyped axonal arbors of retinal ganglion cell subsets in the mouse superior colliculus. *J. Comp. Neurol.* **519**, 1691–1711 (2011).
15. Gale, S. D. & Murphy, G. J. Distinct representation and distribution of visual information by specific cell types in mouse superficial superior colliculus. *J. Neurosci.* **34**, 13458–13471 (2014).
16. Dräger, U. C. & Hubel, D. H. Responses to visual stimulation and relationship between visual, auditory, and somatosensory inputs in mouse superior colliculus. *J. Neurophysiol.* **38**, 690–713 (1975).
17. Meredith, M. A. & Stein, B. E. Interactions among converging sensory inputs in the superior colliculus. *Science* **221**, 389–391 (1983).
18. Cohen, J. D., Hirata, A. & Castro-Alamancos, M. A. Vibrissa sensation in superior colliculus: wide-field sensitivity and state-dependent cortical feedback. *J. Neurosci.* **28**, 11205–11220 (2008).
19. Cohen, J. D. & Castro-Alamancos, M. A. Behavioral state dependency of neural activity and sensory (whisker) responses in superior colliculus. *J. Neurophysiol.* **104**, 1661–1672 (2010).
20. Furigo, I. C. et al. The role of the superior colliculus in predatory hunting. *Neuroscience* **165**, 1–15 (2010).
21. Favaro, P. D. et al. The influence of vibrissal somatosensory processing in rat superior colliculus on prey capture. *Neuroscience* **176**, 318–327 (2011).
22. Allen, W. E. et al. Thirst-associated preoptic neurons encode an aversive motivational drive. *Science* **357**, 1149–1155 (2017).
23. Boyden, E. S., Zhang, F., Bamberg, E., Nagel, G. & Deisseroth, K. Millisecond-timescale, genetically targeted optical control of neural activity. *Nat. Neurosci.* **8**, 1263–1268 (2005).
24. Park, S. G. et al. Medial preoptic circuit induces hunting-like actions to target objects and prey. *Nat. Neurosci.* **21**, 364–372 (2018).
25. Tervo, D. G. et al. A designer AAV variant permits efficient retrograde access to projection neurons. *Neuron* **92**, 372–382 (2016).
26. Westby, G. W., Keay, K. A., Redgrave, P., Dean, P. & Bannister, M. Output pathways from the rat superior colliculus mediating approach and avoidance have different sensory properties. *Exp. Brain Res.* **81**, 626–638 (1990).
27. Shang, C. et al. Brain circuits. A parvalbumin-positive excitatory visual pathway to trigger fear responses in mice. *Science* **348**, 1472–1477 (2015).
28. Gunaydin, L. A. et al. Natural neural projection dynamics underlying social behavior. *Cell* **157**, 1535–1551 (2014).
29. Li, Y. et al. Hypothalamic circuits for predation and evasion. *Neuron* **97**, 911–924.e5 (2018).
30. Coizet, V. et al. Short-latency visual input to the subthalamic nucleus is provided by the midbrain superior colliculus. *J. Neurosci.* **29**, 5701–5709 (2009).
31. Watson, G. D., Smith, J. B. & Alloway, K. D. The zona incerta regulates communication between the superior colliculus and the posteromedial thalamus: implications for thalamic interactions with the dorsolateral striatum. *J. Neurosci.* **35**, 9463–9476 (2015).

32. Kita, T., Shigematsu, N. & Kita, H. Intralaminar and tectal projections to the subthalamus in the rat. *Eur. J. Neurosci.* **44**, 2899–2908 (2016).
33. Mitrofanis, J. Some certainty for the "zone of uncertainty"? Exploring the function of the zona incerta. *Neuroscience* **130**, 1–15 (2005).
34. Fife, K. H. et al. Causal role for the subthalamic nucleus in interrupting behavior. *eLife* **6**, e27689 (2017).
35. Govorunova, E. G., Sineshchekov, O. A., Janz, R., Liu, X. & Spudich, J. L. Natural light-gated anion channels: a family of microbial rhodopsins for advanced optogenetics. *Science* **349**, 647–650 (2015).
36. Zhang, X. & van den Pol, A. N. Rapid binge-like eating and body weight gain driven by zona incerta GABA neuron activation. *Science* **356**, 853–859 (2017).
37. Zhao, Z.-d. et al. Zona incerta GABAergic neurons integrate prey-related sensory signals and induce an appetitive drive to promote hunting. *Nat. Neuro.* https://doi.org/10.1038/s41593-019-0404-5 (2019).
38. Roseberry, T. K. et al. Cell-type-specific control of brainstem locomotor circuits by basal ganglia. *Cell* **164**, 526–537 (2016).
39. Caggiano, V. et al. Midbrain circuits that set locomotor speed and gait selection. *Nature* **553**, 455–460 (2018).
40. Comoli, E. et al. Segregated anatomical input to sub-regions of the rodent superior colliculus associated with approach and defense. *Front. Neuroanat.* **6**, 9 (2012).
41. Meredith, M. A. & Stein, B. E. Descending efferents from the superior colliculus relay integrated multisensory information. *Science* **227**, 657–659 (1985).
42. Stein, B. E. & Meredith, M. A. Multisensory integration. neural and behavioral solutions for dealing with stimuli from different sensory modalities. *Ann. NY Acad. Sci.* **608**, 51–65 (1990).
43. Kleinfeld, D., Ahissar, E. & Diamond, M. E. Active sensation: insights from the rodent vibrissa sensorimotor system. *Curr. Opin. Neurobiol.* **16**, 435–444 (2006).
44. Urbain, N. & Deschênes, M. Motor cortex gates vibrissal responses in a thalamocortical projection pathway. *Neuron* **56**, 714–725 (2007).
45. Liu, K. et al. Lhx6-positive GABA-releasing neurons of the zona incerta promote sleep. *Nature* **548**, 582–587 (2017).
46. Han, W. et al. Integrated control of predatory hunting by the central nucleus of the amygdala. *Cell* **168**, 311–324.e18 (2017).
47. Ricardo, J. A. Efferent connections of the subthalamic region in the rat. II. The zona incerta. *Brain Res.* **214**, 43–60 (1981).
48. Evans, D. A. et al. A synaptic threshold mechanism for computing escape decisions. *Nature* **558**, 590–594 (2018).
49. Qiao, H., Li, C., Yin, P. J., Wu, W. & Liu, Z. Y. Human-inspired motion model of the upper limb with fast response and learning ability—a promising direction for robot system and control. *Assem. Autom.* **36**, 97–107 (2016).
50. Yin, P. et al. A novel biologically inspired visual cognition model: automatic extraction of semantics, formation of integrated concepts, and reselection features for ambiguity. *IEEE Trans. Cogn. Dev. Syst.* **10**, 420–431 (2018).

Acknowledgements

The authors thank T. Südhof, K. Deisseroth, L. Luo, M. Luo and M. He for providing the plasmids and mouse lines. They also thank members of the Neuroscience Pioneer Club for valuable discussions. This work was supported by the National Natural Science Foundation of China (31671095, 31422026, 81471311, 31771150 and 91632301) and Startup Funding at NIBS. All data are archived at the NIBS.

Author contributions

P.C. conceived the study. C.S. performed the injections and fiber implantations. C.S., A.L. Z.X. and Y.L. performed the behavioral tests. C.S., Z.X. and A.L. performed the fiber photometry recording. C.S. Z.X., M.H. and A.L. conducted the histological analyses. C.S. and Z.C. performed slice physiology. W.S. and Y.W. provided the reagents. D.L., C.S., A.L., Z.C. and P.C. analyzed the data. P.C. wrote the manuscript.

Competing interests

The authors declare no competing interests.

Additional information

Supplementary information is available for this paper at https://doi.org/10.1038/s41593-019-0405-4.

Reprints and permissions information is available at www.nature.com/reprints.

Correspondence and requests for materials should be addressed to P.C.

Journal peer review information: *Nature Neuroscience* thanks Jennifer Hoy, Daesoo Kim, and the other, anonymous, reviewer(s) for their contribution to the peer review of this work.

Publisher's note: Springer Nature remains neutral with regard to jurisdictional claims in published maps and institutional affiliations.

Methods

Animals. All experimental procedures were conducted following protocols approved by the Administrative Panel on Laboratory Animal Care at the National Institute of Biological Sciences, Beijing (NIBS). The *vGlut2*-IRES-Cre[51], *Gad2*-IRES-Cre[52] and FosTRAP2 (*Fos*-2A-iCreER)[22] mouse lines were imported from the Jackson Laboratory (JAX Mice and Services). The GAD2-GFP mouse line[53] (GENSAT Project at Rockefeller University) was imported from the Mutant Mouse Resource & Research Centers. GAD2-GFP and *vGlut2*-IRES-Cre lines were crossed to obtain double-transgenic mice for analyses of cell-type specificity in the subthalamus. Mice were maintained on a circadian 12-h light–12-h dark cycle with food and water available ad libitum. Mice were housed in groups (3–5 animals per cage) before they were separated 3 days before virus injection. After virus injection, each mouse was housed in one cage for 3 weeks before subsequent experiments. To avoid potential sex-specific differences[4], we only used male mice.

AAV vectors. Two AAV serotypes (AAV-DJ and AAV2-retro) were used. The AAVs are listed in Supplementary Table 1. The plasmids for pAAV-hSyn-ChR2-mCherry (Addgene, no. 26976), pAAV-EF1α-DIO-ChR2-mCherry (no. 20297) and pAAV-EF1α-mCherry-IRES-Cre (no. 55632) were from the Deisseroth Lab. The plasmid for pFUGW-hGtACR1-EGFP (Addgene, no. 67795) was from the Spudich Lab. The plasmids for pAAV-hSyn-EGFP-2A-TeNT, pAAV-hSyn-EGFP, pAAV-EF1α-DIO-EGFP-2A-TeNT and pAAV-EF1α-DIO-EGFP were from the Südhof Lab. The complementary DNA for pAAV-EF1α-DIO-GCaMP6s was from the Kim Lab (Addgene, no. 40753). The viral particles were produced at the NIBS. The produced viral vector titers before dilution were in the range of $0.8–1.5\times10^{13}$ viral particles per ml. The final titer used for AAV injections was 5×10^{12} viral particles per ml.

Stereotaxic injection. Mice were anesthetized with an intraperitoneal injection of tribromoethanol (125–250 mg per kg). Standard surgery was performed to expose the brain surface above the SC, subthalamus and MLR. Coordinates used for SC injection were as follows: bregma −3.60 mm, lateral ± 1.30 mm and dura −1.75 mm. Coordinates used for subthalamus injection were as follows: bregma −2.00 mm, lateral ± 1.50 mm and dura −4.25 mm. Coordinates used for MLR injection were as follows: bregma −4.70 mm, lateral ± 1.30 mm and dura −2.00 mm. The AAVs and CTB-555 were stereotaxically injected using a glass pipette connected to a Nano-liter Injector 201 (World Precision Instruments) at a slow flow rate of 0.15 μl min^{-1} to avoid potential damage to local brain tissue. The pipette was withdrawn at least 20 min after viral injection.

Optical fiber implantation. Thirty minutes after AAV injection, a ceramic ferrule with an optical fiber (for optogenetics: 200 μm in diameter, numerical aperture (NA) of 0.22; for fiber photometry: 230 μm in diameter, NA of 0.37) was implanted with the fiber tip on top of the SC (bregma −3.60 mm, lateral ± 1.30 mm and dura −1.60 mm), subthalamus (bregma −2.00 mm, lateral ± 1.50 mm and dura −3.90 mm) or MLR (bregma −4.70 mm, lateral ± 1.30 mm and dura −1.80 mm). The ferrule was then secured onto the skull with dental cement. After implantation, the skin was sutured, and antibiotics were applied to the surgical wound. The optogenetic and fiber photometry experiments were conducted 3 weeks after optical fiber implantation. For details of experimental designs, see Supplementary Table 2.

Preparation of behavioral tests. After AAV injection and fiber implantation, the mice were housed individually for 3 weeks before the behavioral tests. Before the behavioral tests, they were handled daily by the experimenters for at least 3 days. On the day of the behavioral test, the mice were transferred to the testing room and were habituated to the room conditions for 3 h before the experiments started. The apparatus was cleaned with 20% ethanol to eliminate odor cues from other mice. All behavioral tests were conducted during the same circadian period (13:00–19:00). All behaviors were scored by the experimenters, who were blinded to the animal treatments.

Measurement of predatory hunting. The procedure of the predatory hunting experiment, which is summarized in Supplementary Table 3, was modified from a previously published method[6]. Before the predatory hunting test, the mice went through a 9-day habituation procedure (days H1–H9). On each of the first three habituation days (days H1, H2 and H3), three cockroaches were placed in the home cage (with standard chow) of mice at 14:00. The mice readily consumed the cockroaches within 3 h after cockroach appearance. On days H3, H5, H7 and H9, we initiated 24-h food deprivation at 19:00 by removing chow from the home cage. On days H4, H6 and H8 at 17:00, we let the mice freely explore the arena for 10 min, followed by three trials of hunting practice for the cockroach. After hunting practice, we put the mice back in their home cages and returned the chow at 19:00. On the test day, we let the mice freely explore the arena for 10 min, followed by three trials of predatory hunting. After the tests, the mice were put back in their home cage followed by the return of chow. In some experiments (for example, see Fig. 1g), predatory hunting of the same mice in a satiated state was also measured. Cockroaches were purchased from a merchant at Tao-Bao Online Stores (www.taobao.com).

Before hunting practice or the test, the mice were transferred to the testing room and habituated to the room conditions for 3 h before the experiments started. The arena was cleaned with 20% ethanol to eliminate odor cues from other mice. All behaviors were scored by the experimenters, who were blinded to the animal treatments. Hunting behaviors were measured in an arena (20 cm × 20 cm, square open field) without regular mouse bedding. After entering, the mice explored the arena for 10 min, followed by the introduction of a cockroach. For each mouse, predatory hunting was repeated for three trials. Each trial began with the introduction of prey to the arena. The trial ended when the predator finished ingesting the captured prey. After the mice finished ingesting the prey, debris was removed before beginning a new trial.

The counting of time was initiated once the cockroach was introduced into the arena. Mouse behavior was recorded in the arena using three orthogonally positioned cameras (50 frames per s; Point Grey Research). We used three parameters (latency to hunt, time to capture and frequency of attack) to quantify the efficiency of predatory hunting in mice. Latency to hunt was defined as the time between the introduction of the prey and the first jaw attack from the predator. Time to capture was defined as the time between the introduction of prey and the last jaw attack. Frequency of attack was defined as the number of attacks divided by time to capture. Predatory jaw attacks were carefully identified by replaying the video frame by frame (50 frames per s). The timing of the attacks was marked with yellow lines along with the PPD time course. Data for three trials were averaged. For testing optogenetically evoked predatory hunting and recording of GCaMP signals during predatory hunting, the optical fiber was connected to the implanted ferrule during hunting practice and test runs. A 1-min light-pulse train (5 ms, 10 Hz, 20 mW) delivered in a 1-min on/1-min off pattern was used for optogenetic stimulation of the SC–S pathway.

Hunting-related actions in the absence of prey. Mouse behavior evoked by SC–S pathway activation (10 Hz, 20 mW) in the absence of prey was examined in an arena containing regular corn cob bedding. A high-speed camera (160 frames per s) was used to capture detailed actions of the mouse. After recording, the videos were quantitatively analyzed by measuring the total time spent digging and gnawing the corn cob bedding with and without photostimulation.

Procedure for sensory deprivation. Visual and vibrissal somatosensory deprivation were produced by darkness and whisker trimming, respectively. Eye-lid suturing was not used because this invasive procedure caused stress that disturbed predatory hunting in the mice. The illuminance in the 'dark' arena was ~0.002 lux, which was measured with an illuminance meter (RTR Optoelectronics Technology). Whisker trimming was performed after mice were anesthetized with an intraperitoneal injection of tribromoethanol (125–250 mg per kg). When mice were hunting for prey in the dark arena (0.002 lux), infrared light was used for behavioral analyses.

GtACR1-mediated photoinhibition of GABA$^+$ ZI neurons. AAV-DJ-EF1α-DIO-GtACR1-EGFP was bilaterally injected into the subthalamus of *Gad2*-IRES-Cre mice followed by implantation of optical fibers bilaterally above the injection sites. Three weeks after AAV injection, the mice were subjected to the regular test procedure of predatory hunting. GtACR1-mediated photoinhibition was achieved by laser illumination (473 nm, 20 mW, 15 s on, 15 s off) on GtACR1-expressing GABA$^+$ ZI neurons during predatory hunting or object exploration.

Measurement of defensive behavior and daily food intake. Measurement of defensive behavior triggered by looming visual stimuli was modified from published procedures[54–57]. Defensive behavior was measured in an arena (35 cm × 35 cm, square open field) containing corn cob bedding. No shelter was provided. A standard computer monitor was positioned above the arena for presentation of overhead looming visual stimuli. After entering, the mice explored the arena for 10 min. This was followed by the presentation of three cycles of overhead looming visual stimuli consisting of an expanding dark disk. The visual angle of the dark disk was expanded from 2° to 20° within 250 ms. The luminance values of the dark disk and background were 0.1 cd m^{-2} and 3.6 cd m^{-2}, respectively. Mouse behavior was recorded (50 frames per s; Point Grey Research) by two orthogonally positioned cameras with light-emitting diodes providing infrared illumination. The instantaneous location of the mouse in the arena was measured by a custom-written MATLAB program. The instantaneous locomotion speed was calculated with a 200 ms time-bin. The MATLAB code is available upon request.

To measure the daily food intake of mice with or without synaptic inactivation of the SC–S pathway, each mouse was housed in a single cage for 1 week. Daily food intake was measured by calculating average daily food intake over 7 days.

Measurement of object-exploration behavior. Object-exploration behavior was performed following a previously published protocol[24]. The mice were habituated to the test chamber (25 cm × 25 cm) for 15 min per day over 5 consecutive days before the behavioral test. After the mice entered the test chamber, they were first habituated to the chamber for 15 min to minimize anxiety and stress. Then a styrofoam cube covered with red paper (2.5 cm × 2.5 cm × 2.5 cm) was gently placed

inside the chamber. The nose-poking behaviors were recorded by the horizontal camera and analyzed by a researcher blinded to the conditions of the mice. The latency and the total time of nose poking were used for quantitative analyses. The traces of mouse locomotion and object dislocation were recorded by the overhead cameras and analyzed offline with the software package EthoVision XT 8.5 (Noldus) using its color-tracking feature.

FosTRAP experiment. AAV-DJ-EF1α-DIO-EGFP was unilaterally injected into the SC of *Fos-2A*-iCreER mice on day 1. Tamoxifen (Sigma T-5648) was dissolved in corn oil (20 mg ml^{-1}) overnight on a shaker at 37 °C. On day 3, tamoxifen was intraperitoneally injected into the *Fos-2A*-iCreER mice at a dose of 150 mg per kg. Six hours after tamoxifen injection, the mice were either allowed to hunt for cockroaches for 1 h in the home cage (Hunting-TRAP) or without hunting (Control: no Hunting-TRAP). On day 24 (3 weeks after Hunting-TRAP), mice were allowed to hunt for cockroaches for 1 h, followed by perfusion. Coronal sections (bregma −1.06 to −5.02) were collected, evenly space by 200 µm, for immunohistochemistry for EGFP and c-Fos. The procedure for reactivating hunting-associated SC neurons was as follows: on day 1, AAV-DIO-ChR2-mCherry was injected into the SC of FosTRAP2 mice, followed by implantation of an optical fiber above the injection site. On day 3, the mice were subjected to tamoxifen injection and hunting-TRAP. On day 24, the hunting-associated ChR2-expressing SC neurons were photostimulated. The effects of reactivating hunting-associated SC neurons on the hunting efficiency was quantitatively measured.

Visual stimulation and air-puff vibrissal stimulation. A computer program generated a black circle (diameter of 10° or 50°) that moved across the visual receptive field of a recorded single-unit in a temporal to nasal side direction of the mouse at different speeds (4° per s or 32° per s). The visual stimulus was rear-projected on a tangent screen in front of the lateral visual field of the mouse (Supplementary Fig. 13). The luminance values of the black circle and gray background were 0.1 cd m^{-2} and 6.6 cd m^{-2}, respectively. The black circle first appeared stationary outside the receptive field for 2 s. Each sweep of the moving black circle was presented with an interval of at least 15 s between trials to allow the cell to recover from any motion adaptation.

To mimic the somatosensory cues of moving prey, brief air-puffs (50 ms) with different strengths (15 p.s.i. or 30 p.s.i.) were delivered through a metal tube (diameter of 1.5 mm) connected to Picospritzer III. The output of Picospritzer III was controlled by a programmable pulse generator. When delivering air-puffs as vibrissal somatosensory stimuli, the tube was oriented from the temporal to the nasal side of the mouse. The distance between the tube nozzle and the whiskers was ~30 mm. When presenting repetitive air-puff stimuli, the frequency was either 0.5 Hz or 2 Hz. For each unit, 10–15 trials were repeatedly presented to the whiskers, so that an average response was obtained.

Single-unit recording and verification of recording sites. The antidromic activation strategy was used to identify the single-unit activity of subthalamus-projecting SC neurons. AAV-DJ-EF1α-DIO-ChR2-mCherry was injected into the SC of *vGlut2*-IRES-Cre mice, followed by implantation of an optical fiber above the subthalamus. Three weeks after viral injection, single-unit recording was performed with a tungsten electrode in the SC of head-fixed awake mice. The tungsten electrode was vertically advanced into the lateral SC with a Narishige micromanipulator. The spikes were amplified by a differential amplifier (Model 1800, A-M Systems), digitized (10 kHz) and stored using the software Spike2 (v.7.03). When the single-unit activity was isolated, a train (10 Hz, 1 s) of light stimulations (473 nm, 1 ms, 2 mW) was delivered to test whether the units were from subthalamus-projecting SC neurons. The putative subthalamus-projecting SC neurons were identified by the antidromic spikes evoked by light pulses illuminating ChR2-mCherry$^+$ axon terminals in the subthalamus. Only units with spikes faithfully following the light stimulations with a latency less than 5 ms were further tested for sensory responses. Spike sorting was performed using Spike2 (v.7.03). For a certain train of action potentials, after setting the threshold of the spikes, Spike2 automatically generated the templates and performed the spike-sorting process. The quality of spike clustering was further confirmed by principal component analysis.

The recording sites of the putative subthalamus-projecting SC neurons were marked with electrolytic lesions applied by passing positive currents (40 µA, 10 s) through the tungsten electrode. Under deep anesthesia with urethane, the brain was perfused with saline and PBS containing 4% paraformaldehyde. After performing regular histological procedures, frozen sections were cut at 40 µm in thickness and counterstained with 4,6-diamidino-2-phenylindole (DAPI) for histological verification of the recording sites (Supplementary Fig. 13).

Fiber photometry recording. A fiber photometry system (ThinkerTech) was used for recording GCaMP signals from genetically identified neurons[29]. To induce fluorescence signals, a laser beam from a laser tube (488 nm) was reflected by a dichroic mirror, focused by a ×10 (NA of 0.3) lens and coupled to an optical commutator (Fig. 5a). A 2-m optical fiber (230 µm in diameter, NA of 0.37) guided the light between the commutator and the implanted optical fiber. To minimize photobleaching, the power intensity at the fiber tip was adjusted to 0.02 mW. The GCaMP6s[58] fluorescence was band-pass filtered (MF525-39, Thorlabs) and collected by a photomultiplier tube (R3896, Hamamatsu). An amplifier (C7319, Hamamatsu) was used to convert the photomultiplier tube current output to voltage signals, which were further filtered through a low-pass filter (40 Hz cut-off; Brownlee 440). The analog voltage signals were digitized at 100 Hz and recorded by a Power 1401 digitizer and Spike2 (CED). Two weeks after AAV injection, fiber photometry was used to record GCaMP signals. A flashing light-emitting diode triggered by a 1-s square-wave pulse was simultaneously recorded to synchronize the video and GCaMP signals. For recordings from freely moving mice, mice with optical fibers connected to the fiber photometry system freely explored the arena for 10 min. A cockroach was then introduced into the arena while the GCaMP signals and hunting behaviors were simultaneously recorded. As a non-prey control, a wooden block (3 cm × 8 cm × 3 cm) was placed in the center of the arena. After the experiments, the optical fiber tip sites were histologically examined in each mouse.

Slice physiological recording. Slice physiological recording was performed according to a previously published protocol[59]. Brain slices containing the SC or subthalamus were prepared from adult mice anesthetized with isoflurane before decapitation. Brains were rapidly removed and placed in ice-cold oxygenated (95% O_2 and 5% CO_2) cutting solution (in mM: 228 sucrose, 11 glucose, 26 $NaHCO_3$, 1 NaH_2PO_4, 2.5 KCl, 7 $MgSO_4$ and 0.5 $CaCl_2$). Coronal brain slices (400 µm) were cut using a vibratome (VT 1200S, Leica Microsystems). The slices were incubated at 28 °C in oxygenated artificial cerebrospinal fluid (ACSF (in mM): 119 NaCl, 2.5 KCl, 1 NaH_2PO_4, 1.3 $MgSO_4$, 26 $NaHCO_3$, 10 glucose and 2.5 $CaCl_2$) for 30 min, and were then kept at room temperature under the same conditions for 1 h before transfer to the recording chamber at room temperature. The ACSF was perfused at 1 ml min^{-1}. The acute brain slices were visualized using a ×40 Olympus water immersion lens, differential interference contrast (DIC) optics (Olympus) and a CCD camera. Patch pipettes were pulled from borosilicate glass capillary tubes (Warner Instruments, no. 64-0793) using a PC-10 pipette puller (Narishige). For recording of action potentials (current clamp), pipettes were filled with solution (in mM: 135 K-methanesulfonate, 10 HEPES buffer, 1 EGTA (ethylene glycol tetraacetic acid), 1 Na-GTP, 4 Mg-ATP and 2% neurobiotin (pH 7.4)). For recording of PSCs (voltage clamp), pipettes were filled with solution (in mM: 135 CsCl, 10 HEPES, 1 EGTA, 1 Na-GTP, 4 Mg-ATP (pH 7.4)). The resistance of pipettes varied between 3.0 and 3.5 MΩ. The current and voltage signals were recorded using MultiClamp 700B and Clampex 10 data acquisition software (Molecular Devices). After establishment of the whole-cell configuration and equilibration of the intracellular pipette solution with the cytoplasm, series resistance was compensated to 10–15 MΩ. An optical fiber (200 µm in diameter) was used to deliver light pulses, with the fiber tip positioned 500 µm above the brain slices. The laser power was adjusted to 5, 10, 15 or 20 mW. Light-evoked action potentials from ChR2-mCherry$^+$ neurons in the SC were triggered by a light-pulse train (473 nm, 2 ms, 10 Hz or 50 Hz, 20 mW) synchronized using Clampex 10 data acquisition software (Molecular Devices). Light-evoked PSCs from ChR2-mCherry$^-$ SC or subthalamus neurons were triggered by single light pulses (2 ms) in the presence of 4-aminopyridine (4-AP, 20 µM) and tetrodotoxin (TTX, 1 µM). D-AP5 (50 µM) and 6-cyano-7-nitroquinoxaline-2,3-dione (CNQX, 20 µM) or picrotoxin (50 µM) were perfused with ACSF to examine the neurotransmitter type used by ChR2-mCherry-expressing neurons.

Histological procedures. Mice were anesthetized with isoflurane and sequentially perfused with saline and PBS containing 4% paraformaldehyde. Brains were removed and incubated in PBS containing 30% sucrose until they sank to the bottom. Post-fixation of the brain was avoided to optimize immunohistochemistry of GABA and glutamate. Cryostat sections (40 µm) containing the SC, subthalamus or MLR were collected, incubated overnight with blocking solution (PBS containing 10% goat serum and 0.7% Triton X-100), and then treated with primary antibodies diluted with blocking solution for 3–4 h at room temperature. Primary antibodies used for immunohistochemistry are provided in Supplementary Table 1 and in the Nature Research Reporting Summary. Primary antibodies were washed three times with washing buffer (PBS containing 0.7% Triton X-100) before incubation with secondary antibodies (tagged with Cy2, Cy3 or Cy5; dilution 1:500; Life Technologies) for 1 h at room temperature. Sections were then washed three times with washing buffer, stained with DAPI, and then washed with PBS. Sections were transferred onto Super Frost slides and mounted under glass coverslips with mounting media. Sections were imaged using an Olympus VS120 epifluorescence microscope (×10 objective lens) or an Olympus FV1200 laser scanning confocal microscope (×20 and ×60 oil-immersion objective lens). Samples were excited by 488, 543 or 633 nm lasers in sequential acquisition mode to avoid signal leakage. Saturation was avoided by monitoring the pixel intensity with Hi-Lo mode. Confocal images were analyzed using the software ImageJ.

Cell counting strategies. Cell counting strategies are summarized in Supplementary Table 4. For counting cells in the SC, we collected 40-µm coronal

sections from bregma −3.28 to bregma −4.48. Six sections evenly spaced by 200 μm were sampled for immunohistochemistry to label cells positive for different markers. We acquired confocal images (×20 objective, Olympus FV1200 microscope) within intermediate and deep layers of the SC followed by cell counting using ImageJ. We calculated the percentages of glutamate$^+$ and GABA$^+$ neurons in the neuronal population retrogradely labeled by CTB-555. For counting cells in the ZI and STN, we collected coronal sections (40 μm) from bregma −1.50 to bregma −2.70. Six sections evenly spaced by 200 μm were sampled for immunohistochemistry to label ZI and STN cells positive for different markers. All six coronal sections contained the ZI, whereas four sections contained the STN. After image acquisition, we outlined the ZI and STN within the subthalamus, followed by cell counting using ImageJ. The boundary between the ZI and STN in coronal sections was identified based on DAPI staining and their distinct cell-type specificity. We calculated the percentages of glutamate$^+$ and GABA$^+$ neurons in NeuN$^+$ populations. For counting cells in the MLR, we collected 40-μm coronal sections from bregma −4.36 to bregma −4.96 for each mouse. Three sections evenly spaced by 200 μm were sampled for immunohistochemistry to label cells positive for different markers.

Data quantification and statistical analyses. Data collection and analyses were performed blinded to the conditions of the experiments. For statistical analyses of the experimental data, two-sided Student's *t*-test and one-way analysis of variance were used. The *n* used for these analyses represents the number of mice or cells. Detailed information on statistical analyses is provided in the figure legends and in Supplementary Table 5.

Reporting Summary. Further information on research design is available in the Nature Research Reporting Summary linked to this article.

Data availability

The data that support the findings of this study are available from the corresponding author upon request.

Code availability

The MATLAB code for data analyses is available from the corresponding author upon request.

References

51. Vong, L. et al. Leptin action on GABAergic neurons prevents obesity and reduces inhibitory tone to POMC neurons. *Neuron* **71**, 142–154 (2011).
52. Taniguchi, H. et al. A resource of Cre driver lines for genetic targeting of GABAergic neurons in cerebral cortex. *Neuron* **71**, 995–1013 (2011).
53. López-Bendito, G. et al. Preferential origin and layer destination of GAD65-GFP cortical interneurons. *Cereb. Cortex* **14**, 1122–1133 (2004).
54. Yilmaz, M. & Meister, M. Rapid innate defensive responses of mice to looming visual stimuli. *Curr. Biol.* **23**, 2011–2015 (2013).
55. Wei, P. et al. Processing of visually evoked innate fear by a non-canonical thalamic pathway. *Nat. Commun.* **6**, 6756 (2015).
56. Huang, L. et al. A retinoraphe projection regulates serotonergic activity and looming-evoked defensive behaviour. *Nat. Commun.* **8**, 14908 (2017).
57. Shang, C. et al. Divergent midbrain circuits orchestrate escape and freezing responses to looming stimuli in mice. *Nat. Commun.* **9**, 1232 (2018).
58. Chen, T. W. et al. Ultrasensitive fluorescent proteins for imaging neuronal activity. *Nature* **499**, 295–300 (2013).
59. Liu, Z. et al. IGF1-dependent synaptic plasticity of mitral cells in olfactory memory during social learning. *Neuron* **95**, 106–122.e5 (2017).

nature research

Corresponding author(s): Peng Cao

Last updated by author(s): Feb 7, 2019

Reporting Summary

Nature Research wishes to improve the reproducibility of the work that we publish. This form provides structure for consistency and transparency in reporting. For further information on Nature Research policies, see Authors & Referees and the Editorial Policy Checklist.

Statistics

For all statistical analyses, confirm that the following items are present in the figure legend, table legend, main text, or Methods section.

n/a	Confirmed	
☐	☒	The exact sample size (*n*) for each experimental group/condition, given as a discrete number and unit of measurement
☐	☒	A statement on whether measurements were taken from distinct samples or whether the same sample was measured repeatedly
☐	☒	The statistical test(s) used AND whether they are one- or two-sided *Only common tests should be described solely by name; describe more complex techniques in the Methods section.*
☒	☐	A description of all covariates tested
☐	☒	A description of any assumptions or corrections, such as tests of normality and adjustment for multiple comparisons
☐	☒	A full description of the statistical parameters including central tendency (e.g. means) or other basic estimates (e.g. regression coefficient) AND variation (e.g. standard deviation) or associated estimates of uncertainty (e.g. confidence intervals)
☐	☒	For null hypothesis testing, the test statistic (e.g. *F*, *t*, *r*) with confidence intervals, effect sizes, degrees of freedom and *P* value noted *Give P values as exact values whenever suitable.*
☒	☐	For Bayesian analysis, information on the choice of priors and Markov chain Monte Carlo settings
☒	☐	For hierarchical and complex designs, identification of the appropriate level for tests and full reporting of outcomes
☒	☐	Estimates of effect sizes (e.g. Cohen's *d*, Pearson's *r*), indicating how they were calculated

Our web collection on statistics for biologists contains articles on many of the points above.

Software and code

Policy information about availability of computer code

Data collection	Fiber photometry: commercialized software from ThinkerTech. Single-unit data: commercialized Spike2 Software Version 7.03. Whole-cell recording data: Commercialized Software Clampex 10.5.
Data analysis	Origin 6.0 Professional, MatLab R2014A; ImageJ (FIJI) (version 2.0.0); Clampfit 10.5; EthoVision XT 8.5 software package; Spike2 Software Version 7.03; Custom code to analyze defensive behavior. Custom code is available upon request.

For manuscripts utilizing custom algorithms or software that are central to the research but not yet described in published literature, software must be made available to editors/reviewers. We strongly encourage code deposition in a community repository (e.g. GitHub). See the Nature Research guidelines for submitting code & software for further information.

Data

Policy information about availability of data

All manuscripts must include a data availability statement. This statement should provide the following information, where applicable:

- Accession codes, unique identifiers, or web links for publicly available datasets
- A list of figures that have associated raw data
- A description of any restrictions on data availability

The data, plasmids and Matlab code generated in this study are available from the corresponding authors upon request.

Field-specific reporting

Please select the one below that is the best fit for your research. If you are not sure, read the appropriate sections before making your selection.

☒ Life sciences ☐ Behavioural & social sciences ☐ Ecological, evolutionary & environmental sciences

Life sciences study design

All studies must disclose on these points even when the disclosure is negative.

Sample size	No sample size calculation was performed. Mouse behavior data for each condition were sampled from 7-8 mice. Slice physiology data for each condition were sampled from 7-8 recorded cells of 3 mice. Immunohistochemical data for each condition were sampled from tissue sections of 3-5 mice. The sample sizes are similar to those reported in previous studies (PMID: 29581428, PMID: 28683263, PMID: 26113723)
Data exclusions	No data were not excluded from the analysis.
Replication	Data of each experiment were acquired and analyzed by two different experimenters blind to the group allocation of the samples. For example, experimenter #1 acquired data set #1 and experimenter #2 acquired data set #2. Then experimenter #1 analyzed data set #2, whereas experimenter #2 analyzed data set #1, totally without knowing which is control or test group. And their results were compared to make sure the results were reproducible.
Randomization	No randomization was used.
Blinding	All investigators were blinded to group allocation during data collection and analysis.

Reporting for specific materials, systems and methods

We require information from authors about some types of materials, experimental systems and methods used in many studies. Here, indicate whether each material, system or method listed is relevant to your study. If you are not sure if a list item applies to your research, read the appropriate section before selecting a response.

Materials & experimental systems

n/a	Involved in the study
☐	☒ Antibodies
☒	☐ Eukaryotic cell lines
☒	☐ Palaeontology
☐	☒ Animals and other organisms
☒	☐ Human research participants
☒	☐ Clinical data

Methods

n/a	Involved in the study
☒	☐ ChIP-seq
☒	☐ Flow cytometry
☒	☐ MRI-based neuroimaging

Antibodies

Antibodies used	Rabbit Polyclonal Anti-EGFP: Abcam, CAT# ab290; Lot# GR3196305-l; dilution 1:2000 Rabbit Polyclonal Anti-Glutamate: Sigma, CAT# G6642; Lot# 116H4815; dilution 1:500 Rabbit Polyclonal Anti-GABA: Sigma, CAT# A2052; Lot# 238K2568; dilution 1:500 Mouse monoclonal Anti-NeuN: Millipore, CAT# MAB377; Lot# A60; dilution 1:2000 Rabbit monoclonal Anti-Fos: Cell Signaling Technology, CAT# 2250; Lot# 10; dilution 1:1000
Validation	EGFP: Website states the rabbit polyclonal anti-GFP antibody (ab290) has been tested in flow cytometry, IHC, ICC, IP, and WB and is suitable for ChIP. Reference: PubMed:30510196 Glutamate: Website states the antiserum is evaluated for activity and specificity by dot-blot immunoassay. The antiserum recognizes L-glutamic acid immobilized on an affinity membrane. No cross-reaction is observed with L-aspartic acid, L-glutamine, L-asparagine, and L-alanine. Reference: PubMed 29581428 GABA: Website states expression of GABA in neucortical cells harvested from the brains of E19 day old rat embyros was detected by immunofluorescence using rabbit anti-GABA antibody. Reference: PubMed 29581428 NeuN: Website states anti-NeuN Antibody, clone A60 detects level of NeuN and has been published and validated for use in FC, IC, IF, IH, IH(P), IP and WB. Reference: PubMed 21496647 Fos: Website states this antibody detects endogenous levels of total c-Fos protein. The antibody does not cross-react with other Fos proteins, including FosB, FRA1 and FRA2. Species Reactivity: Human, Mouse, Rat. Reference: PubMed 29934532

Animals and other organisms

Policy information about studies involving animals; ARRIVE guidelines recommended for reporting animal research

Laboratory animals	Cockroaches (Periplaneta americana) were also used. C57BL/6 male mice (3-5 month old) were used in this study: vGlut2-ires-Cre, GAD2-ires-Cre and FosTRAP2 (Fos-2A-iCreER)

	mouse lines were imported from the Jackson Laboratory (JAX Mice and Services). GAD2-GFP mouse line (GENSAT Project at Rockefeller University) was imported from MMRRC.
Wild animals	No wild animals were used in this study.
Field-collected samples	No field-collected samples were used in this study.
Ethics oversight	All experimental procedures were conducted following protocols approved by the Administrative Panel on Laboratory Animal Care at the National Institute of Biological Sciences, Beijing (NIBS).

Note that full information on the approval of the study protocol must also be provided in the manuscript.